

https://dspace.org/

Mechanical behaviour of microalloyed steels with vanadium forrail axles

Desmond Klenam; Lesley Chown; Malesela Papo; Lesley Cornish

https://hdl.handle.net/10539/45504
DOAJ

Downloaded from a DSpace repository. https://dspace.org/

Hybrid Advances 9 (2025) 100387

Contents lists available at ScienceDirect

Hybrid Advances

journal homepage: www.journals.elsevier.com/hybrid-advances

Research Article

Mechanical behaviour of micro-alloyed steels with vanadium for rail axles

D.E.P. Klenam [a,b,c,*], L.H. Chown [a,b], M.J. Papo [b,d], L.A. Cornish [a,b]

[a] School of Chemical and Metallurgical Engineering, University of the Witwatersrand, Private Bag 3, WITS, 2050, South Africa
[b] DSI-NRF Centre of Excellence in Strong Materials, Hosted by the University of the Witwatersrand, Private Bag 3, WITS, 2050, South Africa
[c] Academic Development Unit, Faculty of Engineering and the Built Environment, University of the Witwatersrand, Private Bag 3, WITS, 2050, South Africa
[d] Advanced Materials Division, Mintek, Private Bag X3015, Randburg, 2125, South Africa

ARTICLE INFO

Keywords:
Ferrite-bainite steels
Rail axle
Hardness
Ultimate tensile strength
Ductility

ABSTRACT

Mechanical and microstructural characterisation after different treatments of three new experimental micro-alloyed steels with vanadium for potential use as rail axles was undertaken. The quenched and tempered alloys had yield strengths from 668-1158 MPa and ultimate tensile strengths (UTS) from 880-1306 MPa. For the normalised and furnace-cooled alloys, the yield strengths were from 389-490 MPa with corresponding ultimate tensile strengths of 679–706 MPa. Although the strengths of the normalised and furnaced-cooled alloys were lower than the quenched and tempered, and the normalised in air alloys, they were higher than most of the standard conventional grades with minimum yield strength of 330 MPa and 600 MPa UTS. The quenched and tempered microstructures were mainly lath martensite and ferrite, with some bainite. All normalised and air-cooled steels, as well as the furnace-cooled 0.13 wt% V and 0.25 wt% V steels, were mainly bainite and ferrite. The normalised and furnace-cooled steels without V had banded ferrite-pearlite. The higher strengths of the quenched and tempered steels were due to the high proportions of martensite and bainite. The normalised and air-cooled and the normalised and furnace-cooled steels showed moderate strengths with elongations between 17% and 19% due to the ferrite-bainite or ferrite-pearlite microstructures. All steels with 0.13–0.25 wt% V had coarse microstructures but showed potential for rail axle applications due to superior mechanical properties than most standard grades.

1. Introduction

There are efforts globally to reduce carbon emissions to 5 gigatons by 2050 [1–4]. This is by developing clean energy initiatives, expanding rail networks, and promoting electric vehicles, which can significantly reduce greenhouse gas emissions. Rail transport is particularly efficient, emitting 75% fewer greenhouse gases than road transport [5,6], with US freight rail contributing less than 0.6% and globally about 2% of transportation emissions [5]. To further enhance sustainability, developing advanced alloys with exceptional properties is essential for reducing emissions in transportation and construction. Railway axles, vital for rolling stock, are typically made from high-strength low-alloy (HSLA) or medium carbon heat-treatable steels [7–13]. High-speed train wagons use HSLA steels, achieving approximately 20% weight reduction without compromising structural integrity and durability due to strengths exceeding 700 MPa [14–16]. Conventional commuter train axles, operating below 160 km/h, are usually produced from medium carbon steels with minimum yield strengths of 330 MPa and ultimate tensile strengths of 600 MPa accordingly to EN 13103, 13104 and 13263 standards [14,15].

The typical working life of a rail axle is ~30 years (10^9 cycles) [13,17,18], and they are expected to achieve ~70% of their life before replacement or recall [19,20]. Axles fail or are considered defective due to surface defects caused by corrosion [21–26], ballast impacts (impingement of small pebbles from the sleeper beds of railway tracks) [20,27–29] and microstructural defects (precipitates and non-metallic inclusions initiating sub-surface cracks [20,21,30–32]. These surface and sub-surface defects become sites for crack initiation during the fluctuating loads which are mainly from dead weight or payloads. Recent changes in climatic conditions and erratic weather have also contributed to defects of these components [33–35]. The dynamic nature of these conditions, e.g., deep cold and heatwaves, can adversely affect the structure and properties, and inadvertently cause premature axle failure [33–35]. Thus, improvement of mechanical properties to promote structural integrity of rail axles is vital.

There has been increased and renewed interest in research and

* Corresponding author. School of Chemical and Metallurgical Engineering, University of the Witwatersrand, Private Bag 3, WITS, 2050, South Africa.
E-mail address: desmond.klenam@wits.ac.za (D.E.P. Klenam).

https://doi.org/10.1016/j.hybadv.2025.100387
Received 26 September 2024; Received in revised form 6 January 2025; Accepted 15 January 2025
Available online 20 January 2025
2773-207X/© 2025 The Authors. Published by Elsevier B.V. This is an open access article under the CC BY license (http://creativecommons.org/licenses/by/4.0/).

development of rail infrastructure for the past two decades [24,33–41]. The European Union modernised and reviewed its recommended guidelines and standard practice for rail axle materials [36,42]. The program ran from 2010 to 2014 under five thematic work packages (WP) focusing on new axle fatigue design methods, new testing methods for rail axle fatigue limit assessment, surface protection technologies, reliability, maintenance and life cycle assessments and cost of mechanical components using non-destructive testing (NDT). Emphasis was on structural integrity of rail axles which required alloys with good mechanical and corrosion properties to be developed [31,36,42]. Critical to the success of the European and global endeavours was the drive for materials with mechanical properties above the minimum required for rail axle applications.

Similar initiatives have been ongoing in various parts of Asia [22,33]. Indian developed corrosion resistant low alloy steels by modifying conventional European standard grades with no addition of Cr, Ni and Mo, while increasing the Mn and Si contents [19,22]. Generally, Cr, Ni and Mo improve mechanical, corrosion, and wear properties, but with increased material cost [43]. The new classes, MS3 and MS6 were designed in 2013 having superior properties than standard European EA1N and EA4T grades with relatively high Si and Mn contents [19,22]. In Korea, fatigue, and tensile properties on typical Mn steel for rail axles have been studied [33]. Recently, ways of improving mechanical properties of rail axle steels by alloying [44], optimizing process parameters [35,41,45] and microstructures [46,47], simulations and numerical modelling of load effect on structural integrity [28] under different environmental conditions [23,47] were carried out. These alloys have better mechanical properties compared to standard steel grades for axle application [21,26,30,48], and can ensure ~70–90 % of the working life of the axles in service.

Africa has much mineral wealth with great potential for functional and structural applications through beneficiation. Structural components in the transportation sector ranging from aerospace, automobile and trains can benefit from this value addition to the mineral wealth. Trains are underutilised in Africa and recent integration of railways into the transport mix has paved way for research [12,43]. This is because mostly rail infrastructure is dilapidated and ~50 % of challenges are material dependent [26]. Materials that are used for mechanical components are country specific and must be responsive or tailor to the atmospheric conditions of that area. This promotes the drive towards mineral beneficiation and value addition to the natural mineral resources.

Vanadium microalloying enhances high-performance low-carbon steels, such as rail axles, by improving their strength, toughness, and overall performance [49–61]. Vanadium forms carbides (VC) that act as nucleation sites during phase transformations, promoting the formation of non-equilibrium phases such as acicular ferrite, bainite and martensite offering excellent combination of high strength and good toughness [56,59,60,62]. It facilitates both grain boundary and intragranular nucleation [49,56,62], resulting in fine grain structures that enhances mechanical properties. Additionally, V influences the transformation from austenite to ferrite and pearlite during controlled rolling and cooling, encouraging bainite formation at low cooling rates and thereby simultaneously increasing strength and toughness [62–65]. The low solute drag coefficient of V in austenite promotes uniform distribution of alloying elements [51], ensuring consistent mechanical properties throughout the material [50,55,56,66]. This homogeneity is crucial for applications requiring high-performance materials, where mechanical properties are not compromised by variations in microstructure. The modification of transformation temperatures and kinetics resulting from V is crucial for optimizing the mechanical properties of low-carbon steels in various structural applications [55,61,66].

Vanadium microalloying enhances the thermal stability of low-carbon steels, especially under severe processing conditions like ECAP [,50,53,67,68]. This enhanced thermal stability is achieved through high dislocation densities and carbon diffusion within the ferrite matrix, which helps maintain mechanical properties for high-temperature applications [64,67,68]. Vanadium also significantly affects strain aging and the preservation of mechanical integrity under cyclic or fluctuating mechanical and thermal stresses [69] and preventing premature failure due to aging effects [64,67,68]. Additionally, the incorporation of vanadium increases resistance to various forms of degradation, including hydrogen embrittlement and corrosion [51,70].

The influence of interstitial C on work hardening of V microalloyed steels varies with strain rate [57,58]. Increasing C reduces work hardening due to enhanced dynamic recovery at low strain rates [58]. At high strain rates, medium carbon steel initially exhibits high work hardening which leads to high flow stress. However, low carbon steels eventually surpass the high flow stress due to the interplay of strain hardening and dynamic softening [58].

Cooling rates significantly influence the mechanical properties of vanadium-microalloyed steels. The toughness–strength combination is driven by the amount of degenerated pearlite, which varies with cooling rates [57,59,71–74]. These steels are characterized by fine MC-type carbides (~5–10 nm) in the ferrite matrix, promoting a Baker-Nutting orientation relationship and specific crystallographic alignment ($[001]_{\alpha}//[001]_{VC}$) [59], thereby enhancing strength and toughness. Rapid cooling lowers the ferrite transformation temperature, increasing nucleation rates and refining ferrite grains through the Hall-Petch effect. It also encourages the formation of non-equilibrium, low-temperature phases such as degenerated pearlite, bainitic ferrite, acicular ferrite or bainite, and martensite – austenite constituents [57,59,71–74], achieving a strength–ductility synergy. Degenerated pearlite are generally formed through cementite nucleation at ferrite/austenite boundaries and the subsequent growth of carbide-free ferrite layers around cementite particles, occurring within the transformation range between normal pearlite and upper bainite [71]. This study presents innovative vanadium-microalloyed steel compositions tailored for rail axle applications by exploring various heat treatments and cooling regimes to engineer desired phases and microstructural features for superior mechanical properties. Additionally, incorporating V content (0.13–0.25 wt%) balances material cost and performance, addressing sustainability goals in alloy development.

2. Materials and experimental procedure

2.1. Sample preparation

Using European standard commercial rail axle steel composition as a baseline [14,16,75], 27 compositions with varying amounts of C, Cr, Ni, Mo, and V were formulated. Thermo-Calc was used to calculate the phase proportions for compositions with different C, Cr, Ni and V contents, using the Thermo-Calc TCFE 5 database. The three compositions selected for casting had cementite phase proportions not more than 4.5 mass %.

A 3 kg rectangular bar was sand cast for each composition (Table 1), pre-heated at 1200 °C and soaked for 30 min until “red heat”. The bars were forged from a thickness of 50 mm–37 mm with a 3T load and were hot rolled to ~25 mm thickness then quenched in water. Square samples (0.4 × 0.4 mm) of the as-rolled alloys were machined for differential scanning calorimetry (DSC) in a Netzsch Simultaneous Thermal Analyser (STA 429 CD/7/G) with a Pt–Rh heating element. The tests were done from 25°C to 1000 °C in air at a heating rate of 5°C/min using alumina crucibles. Each DSC experiment was repeated and averaged. The Ae_3 temperatures and the austenitisation temperatures for subsequent heat treatments were derived by adding 50°C to the data from DSC analyses and the Thermo-Calc results (Table 2). This is to accommodate the possibility of high austenitisation temperature of the alloying elements.

Heat treatments were carried out in a Lenton furnace (with target temperature being ±5°C). The alloys were soaked for 30 min after the full austenitisation temperature was reached. The heat treatments were

Table 1
Compositions of the new steels.

Alloy	Compositions (mass %)									
	C	Si	Mn	P	S	Ni	Cr	Mo	Cu	V
0 %V	0.39	0.29	0.91	0.02	0.02	0.39	0.56	0.19	0.3	0.00
0.13 %V	0.35	0.3	0.8	0.05	0.05	0.40	0.30	0.15	0.3	0.13
0.25 %V	0.33	0.23	0.74	0.01	0.01	0.38	0.51	0.16	0.27	0.25

Table 2
Heat treatment temperatures of the experimental alloys.

Alloy	Ae_3 from Thermo-Calc (°C)	Ae_3 from DSC (°C)	Heat treatment temperature (°C)
0 %V	767	772 ± 12	822
0.13 % V	782	776 ± 10	826
0.25 % V	796	775 ± 15	825

Table 3
Phase names in the Thermo-Calc TCFe5 database for Fe-based alloys.

Phase	Database
Ferrite	BCC_A2
Austenite	FCC_A1#1
M(C,N)	FCC_A1#2

a) normalising and air-cooling, b) normalising and furnace-cooling, and c) oil quenching followed by tempering, where the alloy was heated to 540°C and then allowed to cool.

2.2. Mechanical tests

The 20 × 20 mm samples were sectioned using a water jet cutter and prepared metallographically to 1200 grit for the hardness measurements. Vickers hardnesses were measured at 30 kg testing load with a dwell time of 15–25 seconds according to the ASTM E92 – 17 [76].

Round tensile specimens were machined from the heat treated steels according to the ASTM E8 standard [19] with a gauge length of 25 mm. Tensile tests were done using the ASTM A370-17 standard [19] on an Instron Universal Tensile testing machine with Bluehill software for data acquisition and processing. The tensile tests were conducted in triplicate and results were averaged.

The impact testing was done according to the ASTM E−23 specification. Transverse and longitudinal test specimens were taken according to the EN 13261 specifications [14]. All specimens were tested in room temperature, in triplicate and results were averaged. In terms of the ductile – to – brittle transition temperature (DBTT), impact toughness in the longitudinal direction was measured from −50°C to 200°C. The DBTT curve was plotted, and the lower shelf and upper shelf energies estimated.

2.3. Microstructural characterisation

The as-cast, pre-forged, hot-rolled and heat treated alloys were sectioned and metallographically prepared for microstructural examination. The alloys were etched in 3% Nital for 20–30 s. Microstructures were examined with an Olympus optical microscope with stream image analyser software. Micrographs were taken with an FEI Nova Nano SEM 200 and a Carl Zeiss Sigma FE-SEM with Oxford X-Act EDX detector in both back-scattered electron (BSE) and secondary electron (SE) modes. The fracture surfaces of the tensile test specimens were cut from the samples and ultrasonically cleaned in ethanol for 5 min. The as-cleaned surfaces were then examined in an SEM and images were taken in the BSE and SE modes.

3. Results

3.1. Thermo-Calc simulations

Table 3 shows the common phase names in a TCFe5 steel database and the "#" is assigned to different composition sets of the same structure. Eight phases were calculated for steel with no V (0 wt%) ((Fig. 1 (a)) and 0.13 wt% V alloyed steel with seven for 0.25 wt% V alloy (Fig. 1 (b) and 1 (c)). The six common phases observed for the two new steels were FCC_A1#1, MnS, Liquid, BCC_A2#1, Fe_3C and FCC_A1#2. The two other phases of 0 wt% V were MC_SHP and KSI_Carbide, M_7C_3 and FCC_A1#3 for 0.13 wt% V (Fig. 1 (b)) and an FCC_A1#3 for 0.25 %V alloy (Fig. 1 (c)). Three different FCC phases (FCC_A1#1 and FCC_A1#2, and FCC_A1#3) were calculated in the two alloys with V additions, whereas the FCC_A1#3 phase was absent in the 0 wt% V alloy ((Fig. 1 (a)). As a strong carbide former, V had a strong effect on the phase proportions of the alloys, thus increasing V content decreased the phase proportions of Fe_3C, resulting in increased α-ferrite, KSI_Carbide and FCC_A1#1 (Table 4). The addition of V decreased the cementite proportion by 20% in the 0.13 wt% V steel and 56% in the 0.25 wt% V one and led to ~36–46% increase in the minor phases (FCC_A1#2, MC_SHP, KSI_Carbide and MnS) as shown in Table 4. No discernible trend of the contribution of Cr and Mo was observed on the three steels.

3.2. Mechanical properties

The Vickers hardness values (HV_{30}) of the heat treated new steels are given in Fig. 2. Fast cooling produced high hardnesses. The highest hardnesses were obtained for the rolled and water-quenched and the oil-quenched and tempered steels, whereas the lowest hardness was for the normalised and furnace-cooled steels. A sharp decrease in hardness with increasing V content was observed for the quenched and tempered samples. For the normalised and air-cooled samples, there was a small increase in hardness with increasing V contents, and differences in hardness with increasing V contents were negligible for normalised and furnace-cooled samples.

The stress-strain curves of the heat treated steels are given in Fig. 3. The highest yield and ultimate tensile strengths were obtained for the quenched and tempered 0 wt% V steel (Fig. 3 (a)), whereas the yield and ultimate tensile strengths of the quenched and tempered 0.13 %V and 0.25 %V samples were close to each other. The 0.13 wt% V and 0.25 wt % V normalised, and air-cooled alloys had discontinuous yielding, and wide plastic zones were observed for 0 wt% V and 0.25 wt% V alloys, indicative of high strain (work hardening effects) (Fig. 3 (b)). The stress-strain curves of the normalised and furnace-cooled alloys had larger areas under the curves, showing good toughness (Fig. 3 (c)). The 0.13 wt % V and 0.25 wt% V samples showed discontinuous yielding, whereas the 0 wt% V sample did not.

The yield strength, UTS, elongation and reduction in area of the new steels are given in Table 5. The tensile strengths (yield strength and UTS) increased with increased cooling rate, and the oil-quenched and tempered alloys had the highest values. The 0 wt% V alloy had the highest yield strength and UTS. The normalised and air-cooled 0.13 wt% V alloy had the lowest yield strength and UTS, showing the elongation

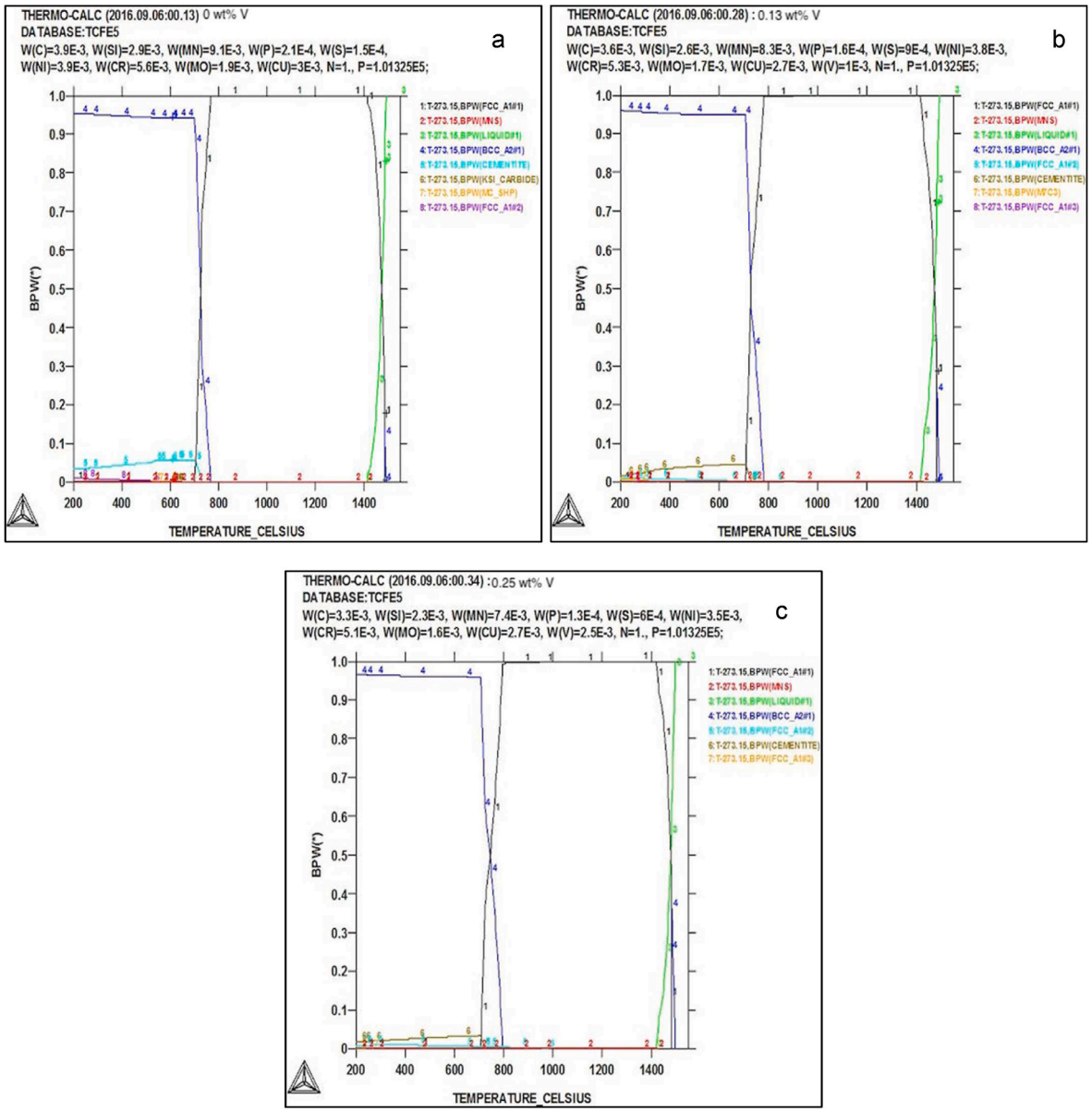

Fig. 1. Phase proportions of low carbon V-microalloyed steels with six common phases as denoted and colour coded as FCC_A1#1 (1), MnS (2), Liquid (3), BCC_A2#1 (4), Fe_3C (5) and FCC_A1#2 (6). The different phases include: (a) KSI_Carbide and MC_SHP for 0 wt% V, (b) M7C3, and FCC_A1#3 for 0.13 wt% V and (c) FCC_A1#3 for 0.25 wt% V.

Table 4
Effect of V on phase proportions of alloys at 400 °C using Thermo-Calc.

Alloy	Mass of phases (%)		
	α-ferrite	Fe_3C	Total minor phases (FCC_A1#2, MC_SHP, KSI_Carbide, MnS)
0 %V	94.71	4.38	0.91
0.13 % V	95.25	3.52	1.23
0.25 % V	96.17	2.46	1.37

and reduction in area decreased with increasing strength. The elongation and reduction in area were below 25% and 55% for all the heat treated alloys.

The impact toughness of the alloys in the transverse and longitudinal sections are given in Fig. 4. Generally, higher impact toughness was observed in the longitudinal direction than the transverse direction. The

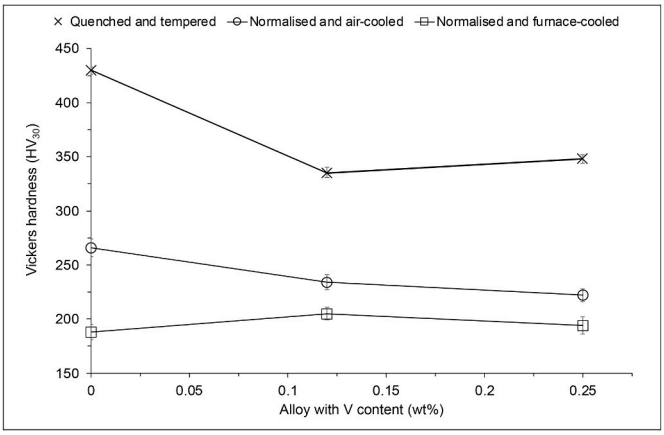

Fig. 2. Vickers hardnesses of the experimental steels.

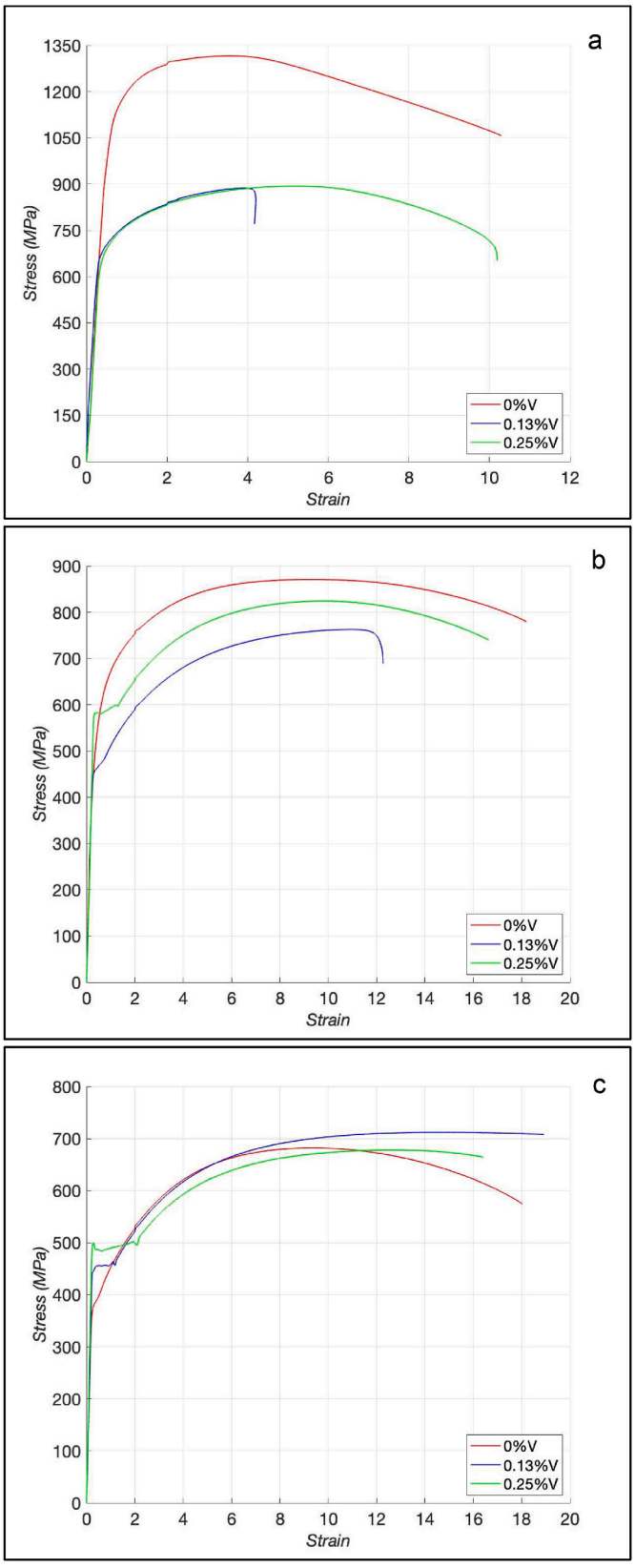

Fig. 3. Stress-strain curves of the heat treated alloys: (a) quenched and tempered, b) normalised and air-cooled and c) normalised and furnace-cooled.

Table 5
Tensile properties of the heat-treated experimental alloys.

Alloy	Yield Strength (MPa)	UTS (MPa)	Reduction in Area (%)	Elongation (%)
Conventional grade [14,15]				
Conventional	≥320	≥550	–	≥22
European standard grades [14,15,77,78]				
EA1N	320	550–650	–	≥22 min
EA4T	420	650–800	–	≥18
30NiCrMoV12	≥834	932–1079	–	≥15
Indian grades [22]				
MS3 & MS6	≥400	≥625	–	≥22
Quenched and tempered				
0 %V	1158 ± 15	1306 ± 13	36 ± 2	10 ± 2
0.13 %V	698 ± 5	880 ± 4	50 ± 1	4 ± 1
0.25 %V	668 ± 8	894 ± 12	47 ± 2	10 ± 3
Normalised and air-cooled				
0 %V	587 ± 7	880 ± 12	30 ± 4	18 ± 3
0.13 %V	455 ± 16	767 ± 20	42 ± 4	12 ± 2
0.25 %V	572 ± 13	803 ± 15	36 ± 3	17 ± 2
Normalised and furnace-cooled				
0 %V	389 ± 4	684 ± 5	45 ± 2	18 ± 3
0.13 %V	455 ± 6	706 ± 3	47 ± 3	19 ± 2
0.25 %V	490 ± 12	679 ± 7	53 ± 3	17 ± 1

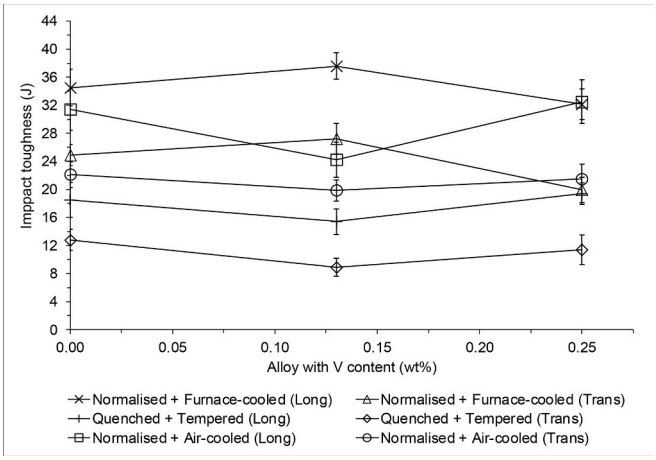

Fig. 4. Longitudinal and transverse impact toughness of the experimental alloys tested at room temperature, where Long = longitudinally-orientated specimen and Trans = transversally-orientated specimen.

toughness of the quenched and tempered alloys was lower than the normalised and air-cooled and the normalised and furnace-cooled, corresponding to the tensile strengths. This is because the higher strength alloys tend to be more brittle, which is the well-known strength-toughness trade-off [79]. Fig. 5 shows the yield strengths and the impact toughness of some conventional and new steels. Some of the data points overlapped due to comparable impact toughness and yield strengths of low alloy carbon rail axle steels. The impact toughness increased with decreasing yield strength as expected. The quenched and tempered steels had the highest yield strengths. Most of the new steels were below the middle range, except for the quenched and tempered 0 wt% V alloy, which was in the top range.

Fig. 6 shows the Charpy V-notch impact toughness tests conducted in the longitudinal direction to determine the ductile-to-brittle transition temperatures (DBTT) ranging from −50°C to 200°C. The results show that the absorbed impact energy decreases as the testing temperature drops, demonstrating the typical behavior associated with the ductile-to-brittle transition. Distinct regions corresponding to the lower shelf energy is between −50°C and 0°C, whereas the upper shelf energy is between 100°C and 200°C. The region where the transition from brittle to ductile fractures ranges between 20°C and 75°C.

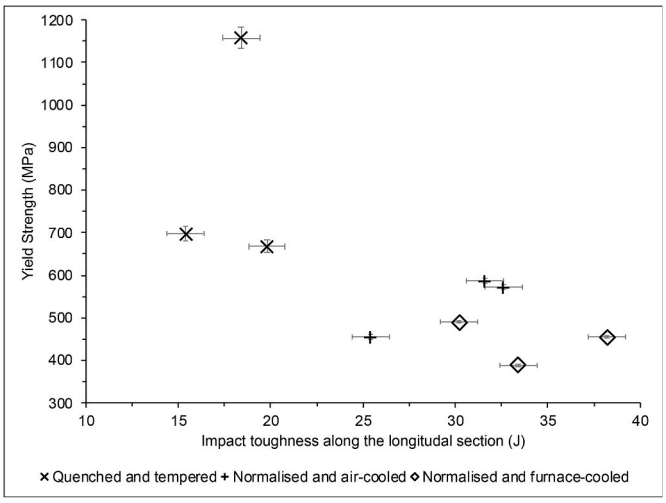

Fig. 5. Relationship between the impact toughness and yield strength of carbon steels.

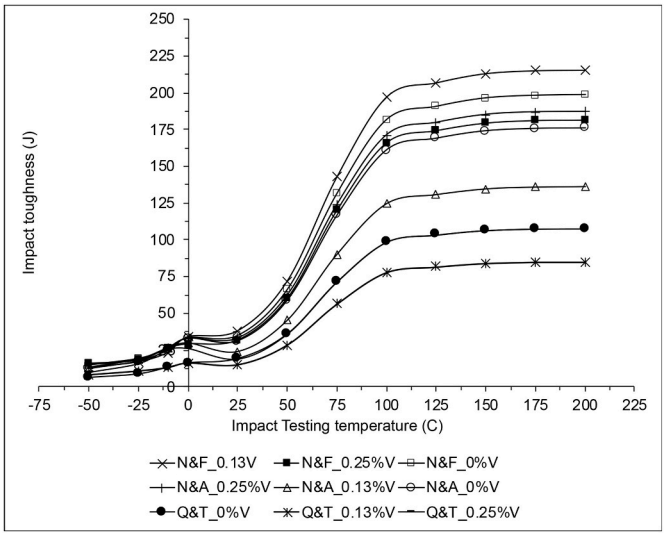

Fig. 6. Ductile – to – brittle-transition (DBTT) of the microalloyed steels under different heat treatment conditions (NB: N&F – Normalising and furnace-cooling, N&A – Normalising and air-cooling and Q&T – Quenching and tempering).

3.3. *Microstructures of the new steels*

The optical and SEM−SE images of the as-cast 0 wt% V and 0.13 wt% V steels are given in Fig. 7. The microstructure was inhomogeneous and had large prior-austenite grains, with some grain boundary pro-eutectoid ferrite for the 0 wt% V steel (Fig. 7 (a)). The microstructure of the as-cast 0.13 wt% V was mainly pearlite with coarse, allotriomorphic pro-eutectoid ferrite at the prior austenite grain boundaries (Fig. 7 (b)). There were pearlite colonies with some blowholes and MnS inclusions, as in the 0 wt% V alloy. Similar microstructural features were observed for the as-cast 0.25 wt% V sample since the compositions were not very different.

All the steels, irrespective of composition, had mainly martensite with some retained austenite after hot rolling and water quenching. There was no discernible difference between the microstructures and a representative microstructure (for 0 wt% V) is given in Fig. 8.

The optical and SEM−SE images of the quenched and tempered steels are given in Fig. 9. The 0 wt% V sample was mainly lath martensite, with some bainite and patches of ferrite (Fig. 9(a)). Similar microstructures of bainite, martensite and ferrite were also observed for the 0.13 wt% V (Fig. 9(c)) and 0.25 wt% V alloys (Fig. 9(e)). The lath martensite of the 0 wt% V was finer than for samples with vanadium. The micrographs (optical and SEM−SE) of the normalised and air-cooled steels are given in Fig. 10, showing well distributed ferrite within the bainite. The optical and SEM−SE images of the normalised and furnace-cooled samples are given in Fig. 11. A coarse ferrite-pearlite microstructure was observed for the 0 %V sample, with banding in the rolling direction (Fig. 11(a)). The 0.13 wt% V and 0.25 wt% V samples showed banded ferrite and bainite (Fig. 11(c)). Finer bainite was observed for the 0.13 wt% V than the 0.25 wt% V sample. The fracture surfaces of quenched and tempered, normalised, and air-cooled and normalised and furnace-cooled samples are given in Fig. 12. Generally, all the samples showed micro-void coalescence and dimples, indicating ductile fracture. Due to the higher strength of the quenched and tempered samples, their dimples were shallower compared to the normalised and air-cooled and normalised and furnace-cooled samples.

Representative EDX analyses which qualitatively show the composition of the 0.13 wt% V steel with the different heat treatment processes are given in Table 6. Although the SEM did not show any minute precipitates, such as inclusions and V-based carbides (because this was beyond the resolution), the EDX area analyses showed V and C, confirming their presence.

4. Discussion

The selection of medium carbon steels for rail axles is driven by cost and strength [22]. Although ferrite-pearlite rail axle steels are the most used for rail axles, micro-alloyed steels with other dual phase microstructures could be an alternative with enhanced properties for structural integrity and for load bearing applications. The alloys studied have the added advantages of good wear and corrosion resistance, which was not initially considered for the ferrite-pearlite steels. The initial standards for rail axles were focused on meeting the strength requirement, relatively heavy and low-cost [7–9,43,80–83]. Initial failure investigations of rail axles focused on fatigue behaviour, which is a strength effect. This necessitated the production of rail axles from hypoeutectoid carbon steels with remarkable strengths but with poor corrosion resistance. The increasing incidents of axle failure due to corrosion required designing against corrosion and corrosion-fatigue of axles.

The as-cast 0 wt% V steel had slightly higher Fe_3C phase proportions (2.46–4.38%) than the as-cast 0.13 wt% V and 0.25 wt% V samples. This was mainly due to V having a higher affinity to carbon than Fe [84], which removed any carbon that could have reacted with Fe. Some carbides other than Fe_3C were calculated by Thermo-Calc, since they comprised slightly stronger carbide formers (V, Cr and Mo) than Fe. Nickel as an austenite stabilizer had no effect on the Fe_3C phase proportions but was added for corrosion resistance [84].

The mechanical properties (strength, hardness, ductility and toughness) of rail axles are essential for structural integrity [17,26,30,85–87]. The strength bears the load, whereas toughness allows some plastic deformation which prevents potential sudden catastrophic failure. The yield and tensile strengths of the micro-alloyed low carbon steels were higher than most conventional rail axle steels (Table 5 and Fig. 3). This was attributed to the alloying elements and the microstructures achieved from the heat treatment (Figs. 9–11). The experimental steels were designed to have mixed microstructures, thus ferrite-bainite, ferrite--pearlite and ferrite-bainite with some prior austenite phase to increase tensile strength and toughness above the recommended standards [14,15,88–91], without compromising the ductility. This allowed for more plastic deformation and increased fatigue life than most conventional rail axle steel grades. This would ensure a more benign ductile failure, and prolonged service life instead of premature and sudden failure driven by defect-assisted failure mechanisms with poor balance of

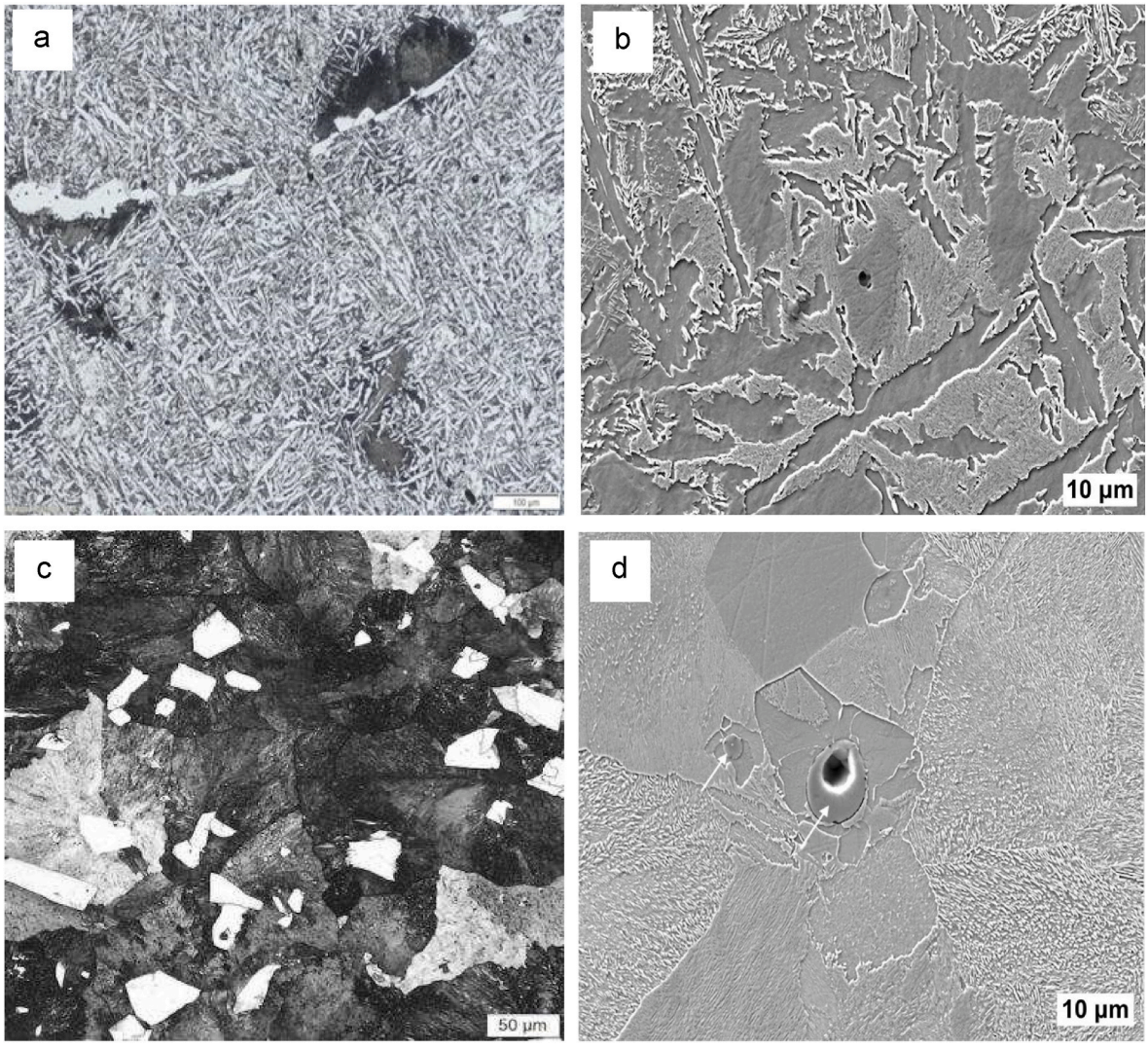

Fig. 7. Images of as-cast samples showing: (a) optical (light needles mainly ferrite) and (b) SEM−SE images of 0 wt% V; (c) optical and (d) SEM−SE image of 0.13 wt % V with ferrite (light) and pearlite (darker) and blowholes (shown by arrow).

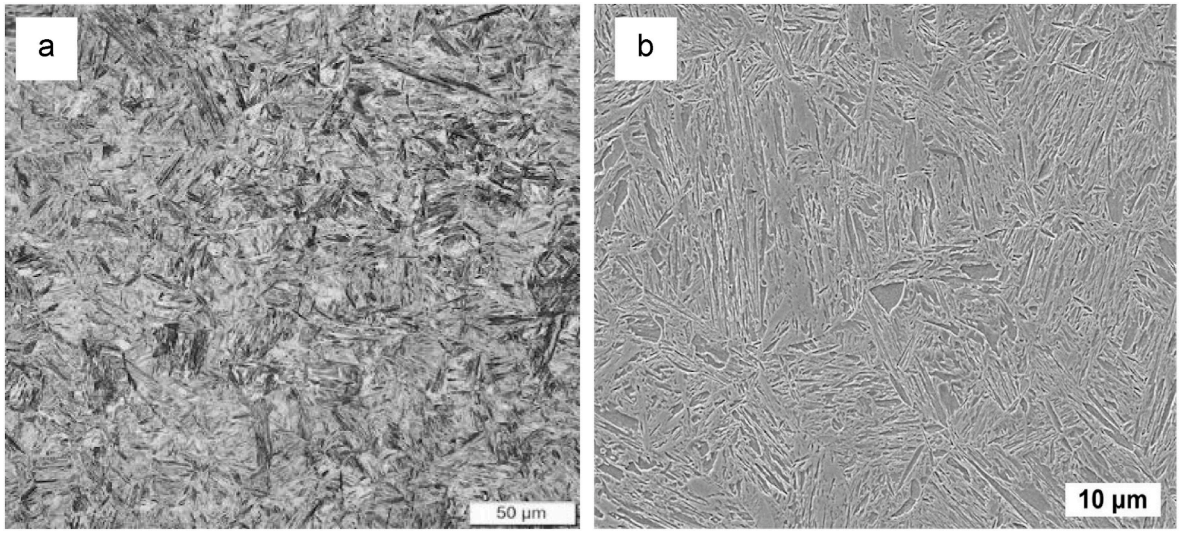

Fig. 8. Images of as-rolled and water-quenched 0 wt% V steel: (a) Optical and (b) SEM−SE, showing martensite.

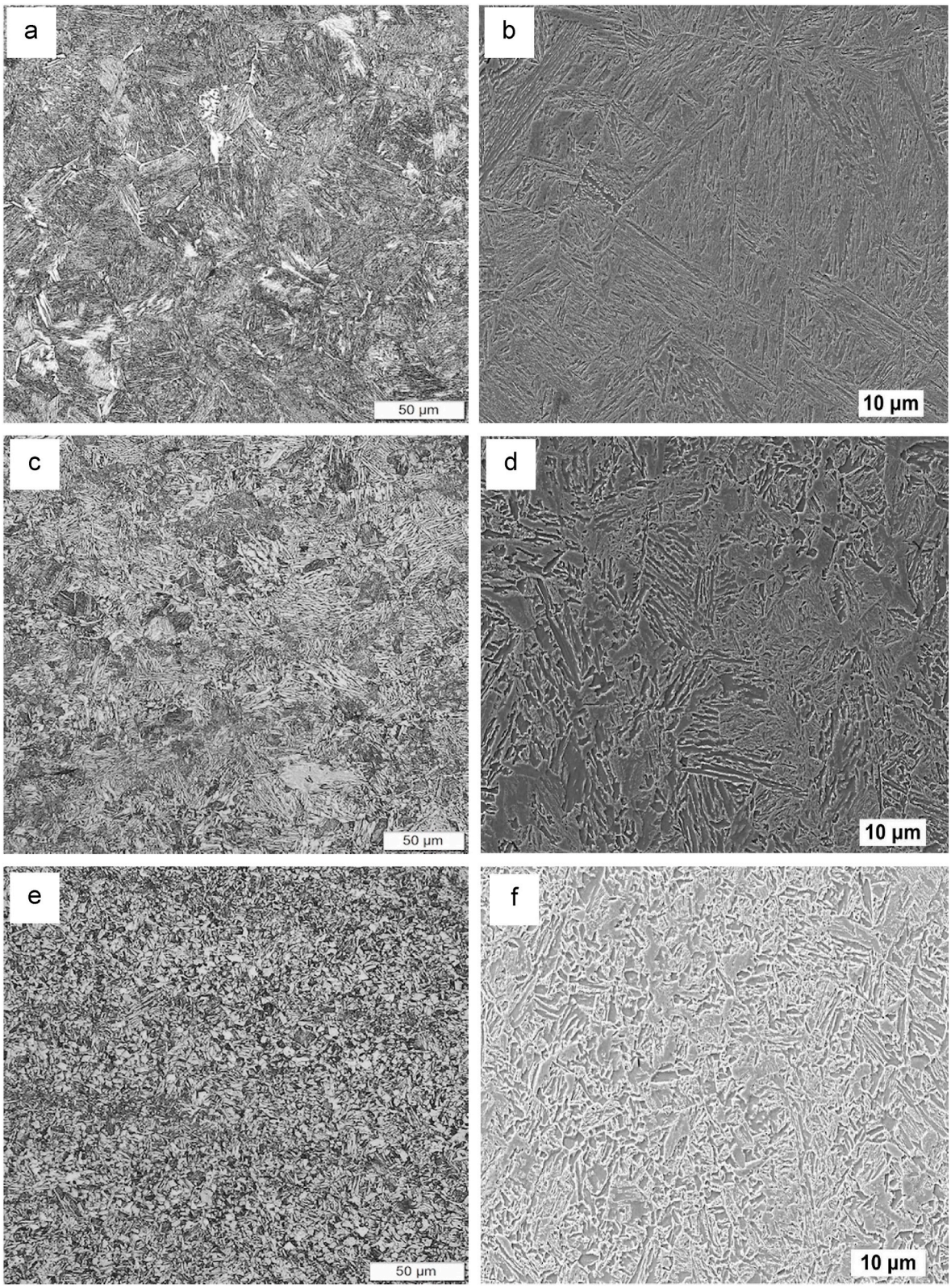

Fig. 9. Optical and SEM−SE images of oil quenched and tempered alloys with: (a and b) 0 wt% V, (c and d) 0.13 wt% V and (e and f) 0.25 wt% V, showing ferrite (light) and bainite (dark).

strength and toughness [20,26]. Alloys with a good balance of strength and toughness have good fatigue life and good fretting wear at the pressed or interference fit [12]. This is shown in Fig. 5 where impact toughness was plotted against the yield strength.

For the micro-alloyed steels, the microstructures strongly affected the mechanical properties. Alloys with ferrite-pearlite and ferrite-bainite microstructures showed appreciable strength and ductility, which is typical for most structural materials where the load bearing ability is the main concern and must be good [14,15,88–93]. In pearlite, the softer ferrite, whether allotriomorphic or Widmanstätten or both,

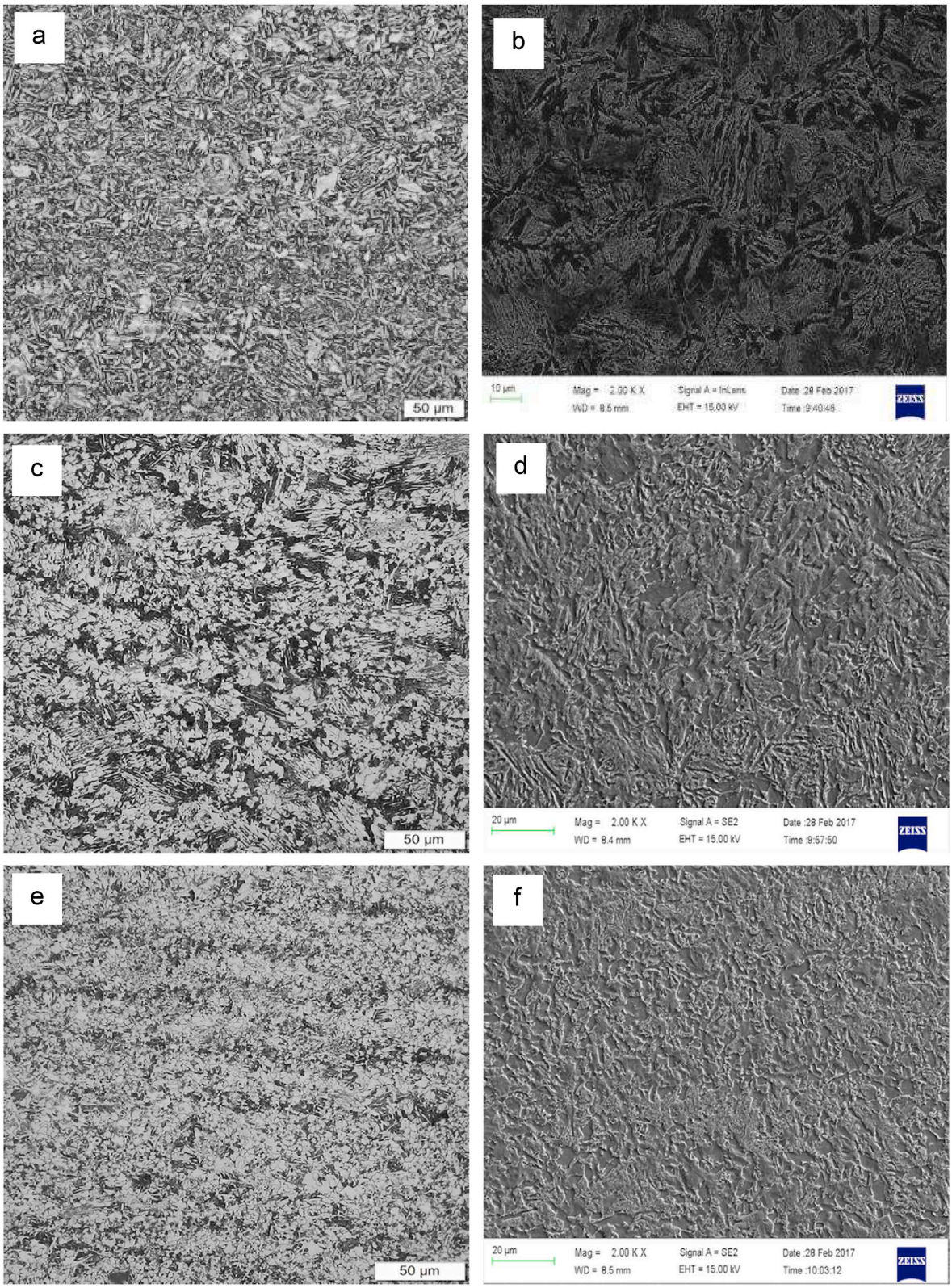

Fig. 10. Optical and SEM−SE images of normalised and air-cooled alloys with: (a and b) 0 wt% V, (c and d) 0.13 wt% V, with c) showing banding and (e and f) 0.25 wt% V, with e) showing banding with mainly ferrite (light) and bainite (dark).

provides the ductility and toughening due to its low inherent strength [19,22,46,94–96]. The cementite, being the harder phase, provides the strength lacking in the ferrite. By ensuring at least 60–40 % of the soft ferrite phase with evenly distributed fine precipitates, inclusions and fine grains in the microstructures, the strength and ductility can be simultaneously improved for rail axle applications [14,15,77,78].

The microstructures of carbon steels are modified by grain refinement by heat treatment, which affects hardness, strength, ductility and toughness [19]. The differences in hardness of the experimental steels were due to the differences in microstructures and compositions. The

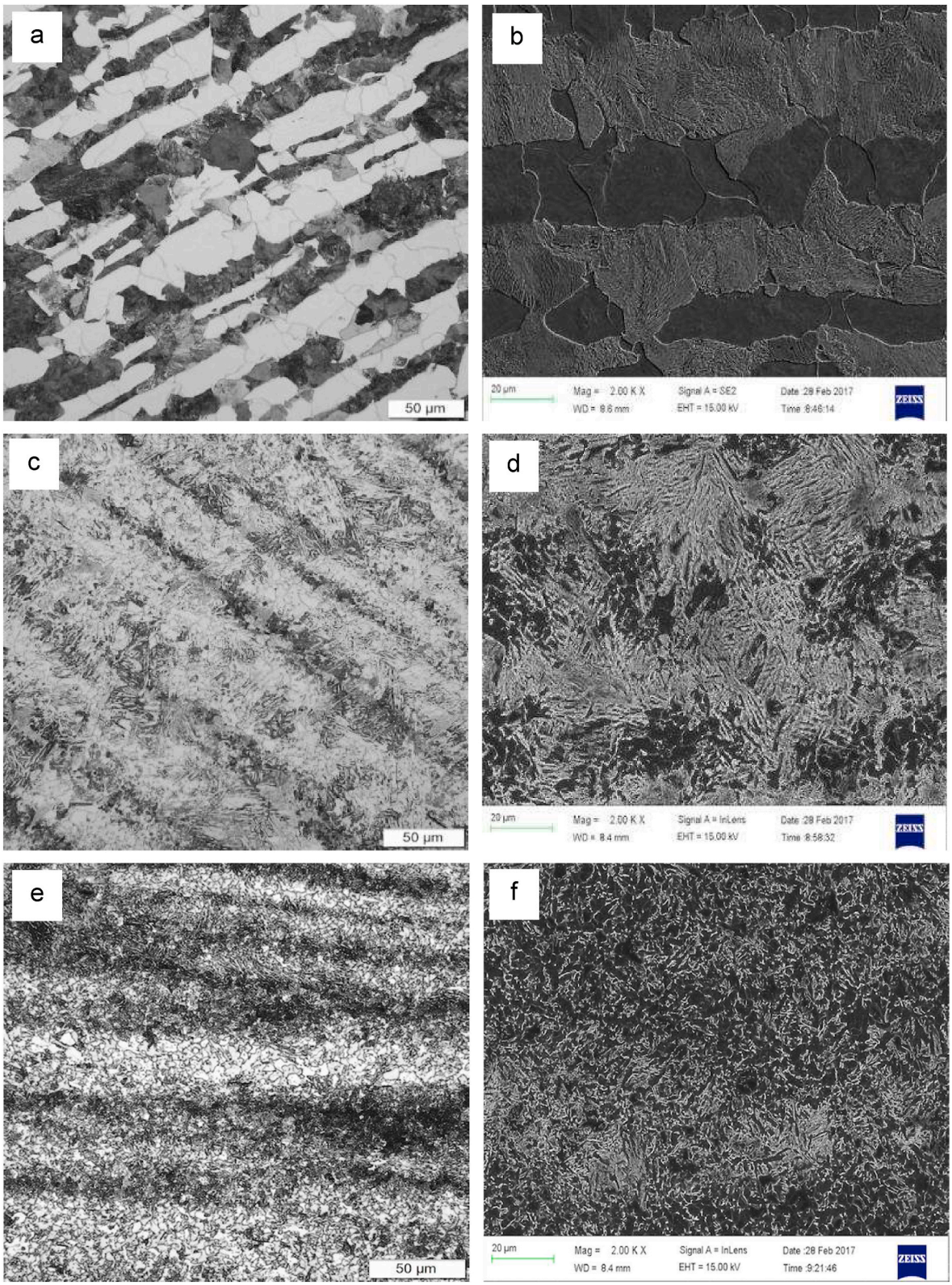

Fig. 11. Optical and SEM−SE images of normalised and furnace-cooled alloys: (a and b) 0 wt% V, (c and d) 0.13 wt% V and (e and f) 0.25 wt% V, showing predominantly ferrite and pearlite with banding along the rolling direction.

highest hardnesses were for the as-rolled and water-quenched steels for all three compositions and were due to the high amounts of lath martensite which increased hardness [97–101]. Thermo-Calc showed the carbide proportion of the 0 wt% V composition was higher than for 0.13 wt% V and 0.25 wt% V compositions (Table 4), so higher hardness was expected for 0 wt% V, which was found experimentally. The higher amounts of C, Cr and Mo in the 0 % V alloy than for 0.13 wt% V and 0.25 wt% V steels gave the higher hardness observed, because of their high affinity for carbon, and hence carbide formation. Carbon in solution is an interstitial atom and its larger size than the interstices create large

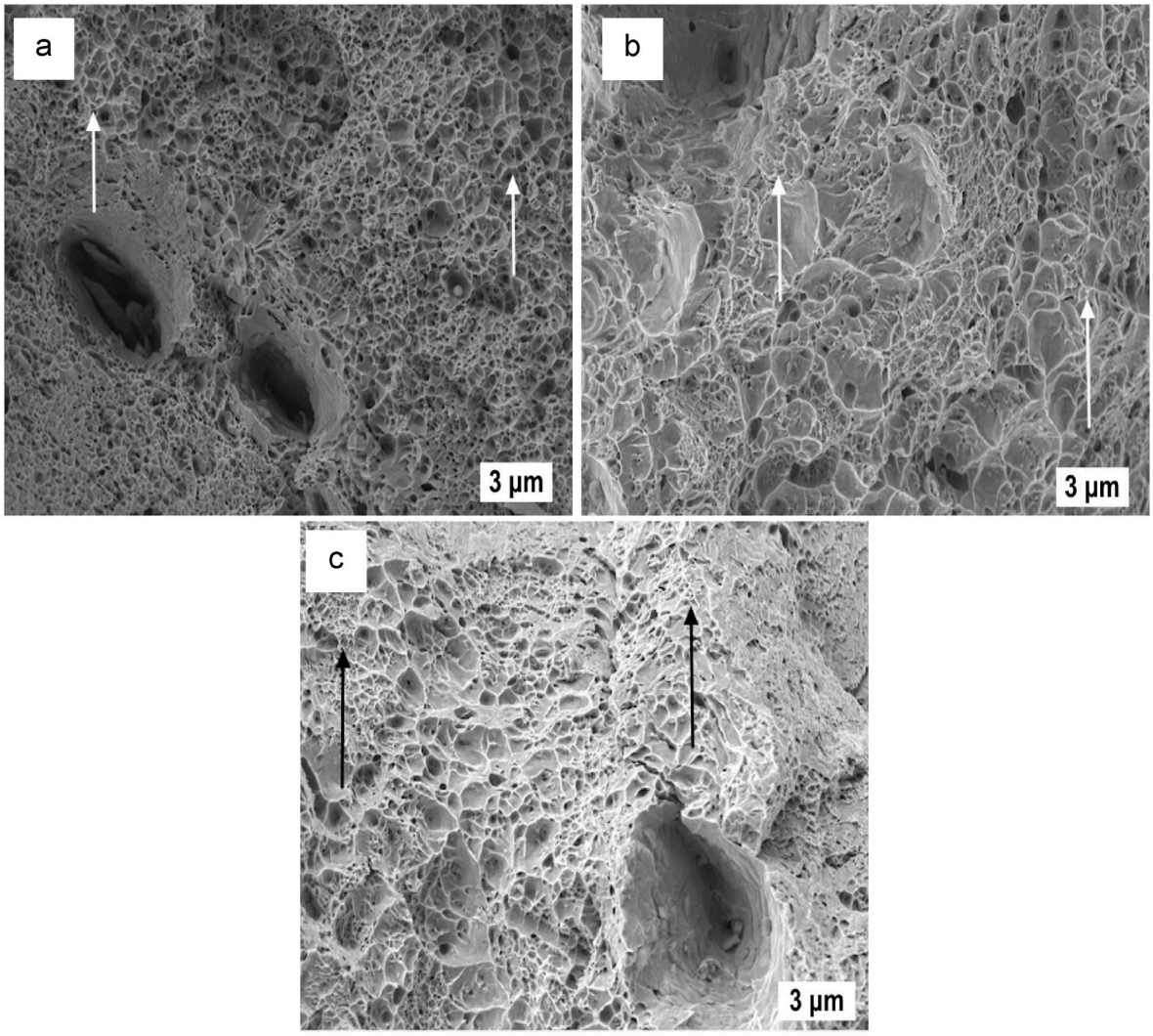

Fig. 12. SEM–SE images of the fracture surfaces of heat treated 0.13 wt% V based samples (arrows showing dimples and micro-void coalescence) for: (a) quenched and tempered, (b) normalised and air-cooled and (c) normalised and furnace-cooled.

Table 6
EDX analyses of 0.13 wt% V based alloys for different heat treatments.

Elements	Quenched and tempered			Normalised and air-cooled			Normalised and furnace-cooled		
	Overall	Ferrite	Bainite	Overall	Ferrite	Bainite	Overall	Ferrite	Bainite
Fe	90.7 ± 0.4	91.6 ± 0.5	91.2 ± 0.7	88.8 ± 2.3	90.3 ± 1.3	89.1 ± 1.7	89.6 ± 2.5	89.2 ± 2.0	89.7 ± 2.5
C	5.6 ± 0.7	5.3 ± 0.3	6.1 ± 0.3	5.4 ± 0.6	5.3 ± 0.3	5.1 ± 0.6	5.1 ± 0.6	5.2 ± 0.8	4.8 ± 0.7
Si	0.4 ± 0.0	0.3 ± 0.0	0.3 ± 0.0	0.6 ± 0.1	0.3 ± 004	0.4 ± 0.0	0.3 ± 0.1	0.2 ± 0.0	0.2 ± 0.0
Cr	0.6 ± 0.0	0.6 ± 0.1	0.5 ± 0.0	1.3 ± 0.7	1.1 ± 0.4	1.5 ± 0.1	1.3 ± 0.5	1.7 ± 0.4	1.2 ± 0.4
Mn	1.1 ± 0.2	0.8 ± 0.1	0.7 ± 0.1	1.5 ± 0.3	1.2 ± 0.3	1.3 ± 0.6	1.4 ± 0.4	1.6 ± 0.5	1.7 ± 0.4
V	0.2 ± 0.0	0.2 ± 0.0	0.4 ± 0.0	0.6 ± 0.1	0.3 ± 0.0	0.5 ± 0.0	0.3 ± 0.1	0.2 ± 0.0	0.4 ± 0.0
Mo	0.6 ± 0.1	0.5 ± 0.0	0.3 ± 0.0	0.6 ± 0.1	0.4 ± 0.0	0.5 ± 0.2	0.4 ± 0.1	0.3 ± 0.0	0.4 ± 0.0
Cu	0.3 ± 0.0	0.3 ± 0.0	0.2 ± 0.0	1.2 ± 0.4	0.9 ± 0.2	1.1 ± 0.3	0.9 ± 0.4	1.1 ± 0.2	0.9 ± 0.2
Ni	0.5 ± 0.1	0.4 ± 0.0	0.3 ± 0.0	0.6 ± 0.0	0.2 ± 0.0	0.5 ± 0.0	0.7 ± 0.3	0.5 ± 0.1	0.7 ± 0.2

displacements with hydrostatic strains with significant volume change that distorts the cubic structure from body centred cubic to body centred tetragonal for martensite [98] and causes the high hardness of martensite. The volume change associated with the martensite transformation is significant enough to induce cracking.

The alloying elements enhanced the mechanical properties of the steels. Carbon promoted interstitial strengthening and increasing the C content to ~0.4 wt% in bainitic steels gave strengths above 1150 MPa [94], which are similar to steels with ferrite-bainite microstructures [102,103]. By keeping C below 0.4 wt% and Mn below 1.0 wt%, toughness was expected to be retained and strength increased [94]. Chromium and Mo are carbide formers and increased the high hardness by precipitation strengthening, grain refinement and increased martensitic transformation temperature [103–105]. Vanadium is added to low alloy steels to improve strength and toughness by preventing grain growth of austenite during heat treatment [94]. However, the steels with 0.13 wt% V and 0.25 wt% V showed well distributed coarse grains (Figs. 10 and 9).

In steels, Cr, V and Fe have strong affinity for C, O and N, and form stable phases of carbides, oxides, and nitrides that pin grain boundaries [64,65,106,107]. However, the SEM images and XRD did not identify the Cr and V carbides which could have been too small to resolve in SEM and below 4 % in volume and so undetectable [108]. Although the carbides were minute, they might not also have had the suitable morphology to pin grain boundaries [109–112]. In low-carbon and heat treatable steels, at least 0.05 wt% V and a carbon content of 0.5 wt% to 1.0 wt% [64,65,107] are needed to enhance strength. Where the C contents are below 0.5 wt%, the contribution of vanadium to precipitation strengthening is negligible [64,65,106,107,113]. In this work, the C contents were 0.33–0.35 wt% with 0.13–0.25 wt% V, so the C contents were below the threshold for noticeable strengthening from V(C,N) precipitates pinning the grain boundaries. Furthermore, there were no vanadium carbides at 400 °C calculated by Thermo-Calc (Fig. 1 and Table 4). This agreed with results for micro-alloyed steels with 0.012–0.102 wt% V which had low or negligible precipitation strengthening from V–based carbides or nitrides [113]. No discernible trends of the influence of V are attributed to the dominance of processing conditions over vanadium effects [64,65,106,107,113]. Slow cooling rates in these steels result in coarse ferrite-bainite or ferrite-pearlite microstructures that overshadow potential vanadium carbide (VC) precipitation strengthening. Additionally, the low carbon content (~0.33–0.35 wt%) is insufficient for significant precipitation strengthening, and thermodynamic limitations, thus insufficient driving force for the nucleation of VC at low cooling rates [64,65,106,107,113]. The lack of significant VC precipitation at 400°C, as predicted from Thermo-Calc supports the observed minimal influence of vanadium on the mechanical behavior of the steels. Generally, ferrite-dominated microstructures exhibit dynamic strain aging (DSA) due to solute atoms like carbon and nitrogen, masking any subtle vanadium contributions. Typical effect of DSA is the serration in the stress-strain curves as shown in Fig. 3(b) and Fig. 3(c). Thus, the vanadium content had minimal impact because its effects were homogenized within the composite microstructures, while cooling rates and carbon content played a more critical role. Nickel increased the carbon content of residual austenite without compromising hardenability [84,94]. It was also added to improve corrosion resistance, which was not the original aim in material selection for rail axles [14,15].

Finer lath martensite and retained austenite in the water-quenched steels than in the oil-quenched and tempered samples also led to their higher hardnesses. The entrapment of C during quenching with the associated distortion and high residual stresses also contributed to the high hardness of the quenched and tempered experimental steels [84,114,115]. However, the lower hardnesses of quenched and tempered samples than the hot rolled and water-quenched samples was because tempering partially redistributed carbon, after it moved out of the martensite. This reduced hardness and strength (Fig. 2) and increased toughness and ductility [84]. Tempering is done after quenching to allow some carbon to diffuse from the martensite [46,84,116,117], which reduces distortion, reduces the proportion of martensite and relieves internal stresses, thus increasing ductility and reducing strength and hardness [118–120]. The lath martensite transformed to bainite and pearlite, which had lower strength than the martensite [121–126].

The normalised and air-cooled and normalised and furnace-cooled samples had lower hardness and strength than the water-quenched and oil-quenched and tempered samples (Fig. 9), due to their ferrite-bainite (Fig. 10) and ferrite-pearlite microstructures (Fig. 11). Slow cooling rates allowed time for the displacive transformation to bainite [84,114,115,121–126], which was observed for all the normalised and air-cooled and the normalised and furnace cooled 0.13 wt% V and 0.25 wt% V samples (Figs. 10 and 11). Although no VC precipitates were visible in optical and SEM images, EDX (Table 6) confirmed they were present, so they were likely to be very small, coherent and finely dispersed and thus too small to be resolved by SEM. Large plastic regions on the stress-strain curves, indicative of high strain or work hardening, occurred for all the normalised and furnace-cooled, and quenched and tempered 0.13 wt% V and 0.25 wt% V alloys (Fig. 3).

Fig. 13 shows that UTS values of the experimental alloys, some conventional axle steel grades which were in a band where high hardnesses had corresponding high strengths, as expected [79]. The differences in strength for the experimental alloys were due to their microstructures, and varied with the proportions of martensite or bainite, both being harder than pearlite. The highest yield strength and UTS of the oil-quenched and tempered 0 wt% V sample were due to the combined effects of lath martensite, bainite and ferrite. The fine laths of bainite and martensite had higher strength than ferrite-pearlite because propagating cracks at the grain boundaries are either arrested or deflected, so more energy is needed to propagate those cracks [121–127], whereas cracks propagate more easily (with less energy) in coarse bainite and martensite.

The lower yield and UTS of the normalised and furnace-cooled 0 wt% V sample were due to the coarse ferrite-pearlite microstructure. Increasing average grain size of the ferrite-pearlite microstructure decreases yield strength according to Hall-Petch relationship [101,]. Banding occurs in hot-rolled low carbon steels and decreases yield strength and UTS [104,128]. Although the yield strength and UTS of the normalised and furnace-cooled steels were the lowest, they were higher than the standard grades being used for rail axles [14,15,77,78], which was due to the selected compositions of the experimental steels. However, since the axles are forged, this would further improve the strength and decrease the ductility [7,8,10,129,130].

With V additions, normalised and furnace-cooled samples and the normalised and air-cooled samples showed discontinuous yielding. This is also known as the Portevin – Le Chatelier effect [131–134] and is due to dynamic strain ageing (interactions between moving dislocations and solute atoms) [98,101,126,135]. The interstitial atoms, such as C, N and O, pin dislocations temporarily [98,101,126,135]. Carbon atoms are a little larger than the sites they occupy in ferrite [43], and with sufficient energy (i.e., heat), carbon atoms tend to diffuse to dislocations where there is lower misfit, reducing local strain [98,101,126,135]. When stress is applied, any dislocation associated with an interstitial carbon requires more stress to move it away from that interstitial atom, giving the upper yield point. A sharp decrease in stress occurs once the dislocation is pulled away from the interstitial carbon atom, because the dislocation is easier to move, giving the lower yield point [98,101,126,135]. Discontinuous yielding is associated with ferrite-pearlite and ferrite-bainite microstructures, which have inherently lower dislocation densities than the martensite and fully bainitic microstructures [98,100,126]. For high dislocation density microstructures, there is no strain accumulation without substantial increase in stress, thus no

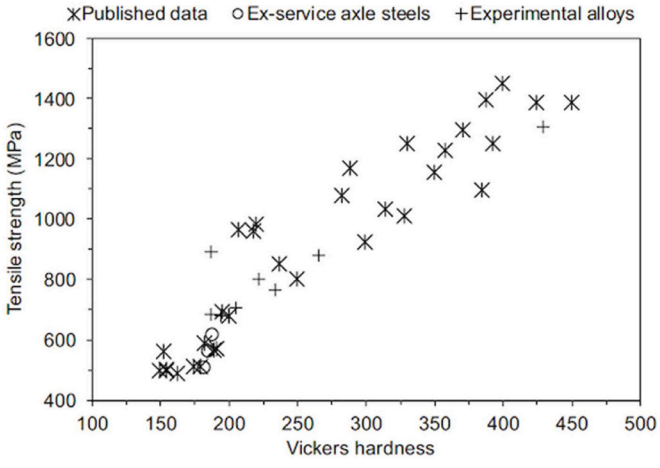

Fig. 13. Ultimate tensile strength as a function of hardness of published rail axle carbon steels [14,15,77,78] compared with the experimental steels.

discontinuous yielding is observed, as for the quenched and tempered samples (Fig. 3(a)).

The strengths of the experimental steels (Table 5) were higher than the standard European grades [14,15,77,78], conventional [14,15] and developed Indian grades [22]. The higher yield and ultimate tensile strengths of the experimental steels were associated with lower elongation (decreased ductility), as expected [79]. The yield and tensile strengths followed the Hall-Petch relationship where decreased grain size promotes higher strength at ambient temperature [136–138]. Small grains have more grain boundary area, and are barriers to dislocation movement, resulting in pile-ups of dislocations [102,105,139–142].

Alloying elements affect strength and toughness of alloys [143–149]. For most low carbon and HSLA steels, there is a trade-off between strength and toughness [13,19,20,22,26,78,150]. These alloys are predominantly Fe with other alloying elements such as Cr, Mo, Ni, Si, P and Mn accounting to 2–5 wt% in total [14,15,77–79]. Although strength and toughness as well as ductility are mutually exclusive in most alloys, they can be balanced by tailoring compositions and controlling heat treatment.

The Charpy V-notch impact toughness results revealed the typical ductile-to-brittle transition behavior of microalloyed steels, influenced by heat treatment conditions (Fig. 6). The ductile-to-brittle transition temperature (DBTT) ranged between −50°C and 200°C, with distinct lower shelf energies observed below 0°C and upper shelf energies above 100°C. The transition from brittle to ductile fracture occurred within 20°C–75°C, highlighting the sensitivity of these steels to temperature changes. Steels subjected to quenching and tempering exhibited lower toughness and higher DBTT values compared to those normalised and furnace – or air – cooled, indicating that the tempered martensitic structure increases strength but compromises toughness. Conversely, the ferrite-bainite microstructures resulting from normalising and air- or furnace-cooling provided a better balance of toughness and ductility, as evidenced by their lower DBTT and higher impact energies. These findings emphasize the critical role of heat treatment in optimizing the mechanical properties of microalloyed steels for applications requiring resistance to low-temperature impacts.

The toughnesses of the experimental alloys were comparable to minimum toughness required for rail axles [13,19,20,22,26,78,150]. Although ductility and toughness were inversely proportional to strength, as observed in most samples, this is mainly driven by alloying elements which define the microstructure [79]. The lowest fracture toughness and Charpy impact energy with the highest transition temperature for micro-alloyed steels occurred for 0.13 wt% V (Fig. 5), above which there was no discernible trend in toughness. In low carbon steels, molybdenum lowers the bainitic transformation temperature (bainite is formed at lower temperatures) contributing to hardenability with overall improvement in strength and toughness [151,152]. The addition of 0.14 wt% Mo contributed to ~400 MPa increase in tensile strength [152]. Therefore, the Mo contents of the experimental steels helped promote the good strength and ductility with high bainite proportions. Similarly, Cr only affects the toughness of low alloy steels above 0.56 wt % Cr (Table 1 and Fig. 4), and increases the continuous cooling transition temperatures in Fe – C based alloys and reduces toughness [153, 154]. Microstructural banding is characteristic of hot-rolled and normalised, air-cooled and furnace-cooled low carbon steels [128,155, 156]. It occurs on rolling where some phases deform more easily than others, due to their structures and segregation of substitutional alloying elements [156]. It also depends on the difference in carbon content across the microstructure. Banding decreases yield and ultimate tensile strength [128,156,157] and was observed for the current alloys under the normalised, air- and furnace-cooled conditions.

Accumulation of plastic deformation in ductile materials leads to fracture. The fracture surfaces of failed alloys are characteristic of the deformation type and can be analysed to identify the failure mechanisms and mechanical behaviour. The fracture surfaces of the 0.13 wt% V heat treated samples (Fig. 12) and the quenched and tempered 0.13 wt% V sample had fewer and more sparsely distributed dimples and microvoids, showing lower ductility than the normalised and air-cooled and furnace-cooled alloys. Small (0.2–5 μm) and large (15–120 μm) dimples were observed on all fracture surfaces. Steels with smaller dimples showed lower ductility than those with larger dimples [138]. The quenched and tempered alloys with characteristic small and shallow dimples had higher tensile strength than alloys that were normalised in the furnace, and air-cooled alloys. The normalised and furnace cooled alloys had better combinations of strength and ductility than the normalised and air-cooled alloys, as indicated by very large dimples (Table 5). The dimple sizes were dependent on the grain sizes (Fig. 14), as observed for heat treatable alloys [138]. A linear relationship was recorded between the size and density of dimples and the grain sizes for metals [138,158–161]. However, coalescence of different sized voids occurs in some materials [161]. The fracture surfaces showed ductile failure with dimples from micro-void coalescence (Fig. 12). These micro-void coalescences are dislocation-induced defects resulting from inclusions and precipitates [135,162]. In yielding (propagation of defects under plastic strain or hydrostatic stresses), these voids stretched and then coalesced to form larger voids and dimples [163]. The ridges between the dimples are usually the last materials to deform.

The experimental normalised and air-cooled, and normalised and furnace-cooled steels had strengths between 679 and 880 MPa with elongations between 17% and 21%, which were higher than the typical European [14,15] and Indian standard grades [19]. Since strength is the main reason for selecting hypo-eutectoid carbon steels with ferrite-pearlite microstructures for rail axle applications [19,22,46], micro-alloyed steels were considered for better axle steels. The normalised, air-cooled, and normalised and furnace-cooled 0 wt% V and 0.13 wt% V steels are recommended as a basis for further optimization because of their overall balanced strength and toughness which are critical for structural integrity. The 0.25 wt% V samples did not show better mechanical properties than the 0 wt% V and 0.13 wt% V, hence the 0.25 wt% V addition was not effective and would unnecessarily increase the material cost [80].

5. Conclusions

The study highlight an improved mechanical properties of the vanadium-microalloyed steels for rail axle applications. Quenched and tempered alloys achieved remarkable yield strengths ranging from 668 MPa to 1158 MPa, and UTS between 880 MPa and 1306 MPa, surpassing the standard rail axle grades such as EA1N and EA4T, which exhibit yield strengths of 320–420 MPa and UTS of 550–800 MPa. The incorporation of vanadium (0.13 wt% and 0.25 wt%) influenced the mechanical behaviour significantly, reducing the cementite content by 20% and 56%, respectively, compared to the non-alloyed steel, thereby enhancing strength and toughness through bainite and ferrite microstructures.

The ductility and toughness of the steels showed a strength-toughness synergy, with elongation values between 17% and 19% in the normalised and furnace-cooled microalloyed steels. These values were higher than the ~15% elongation typically reported for conventional grades. Additionally, the quenched and tempered steels, despite their higher strengths, maintained reasonable toughness with microstructures predominantly comprising lath martensite and bainite. The reduction in area measurements, ranging from 36% to 53%, further underscored the mechanical balance achieved in the micro-alloyed compositions.

Impact toughness varied between the transverse and longitudinal orientations, with longitudinal toughness generally being superior, as demonstrated by Charpy V-notch tests. The highest impact toughness was observed in normalised and furnace-cooled steels, correlating to their ferrite-bainite microstructure, which provides a moderate balance of strength and toughness. Notably, the inclusion of 0.25 wt% V did not yield proportional improvements in mechanical properties, suggesting

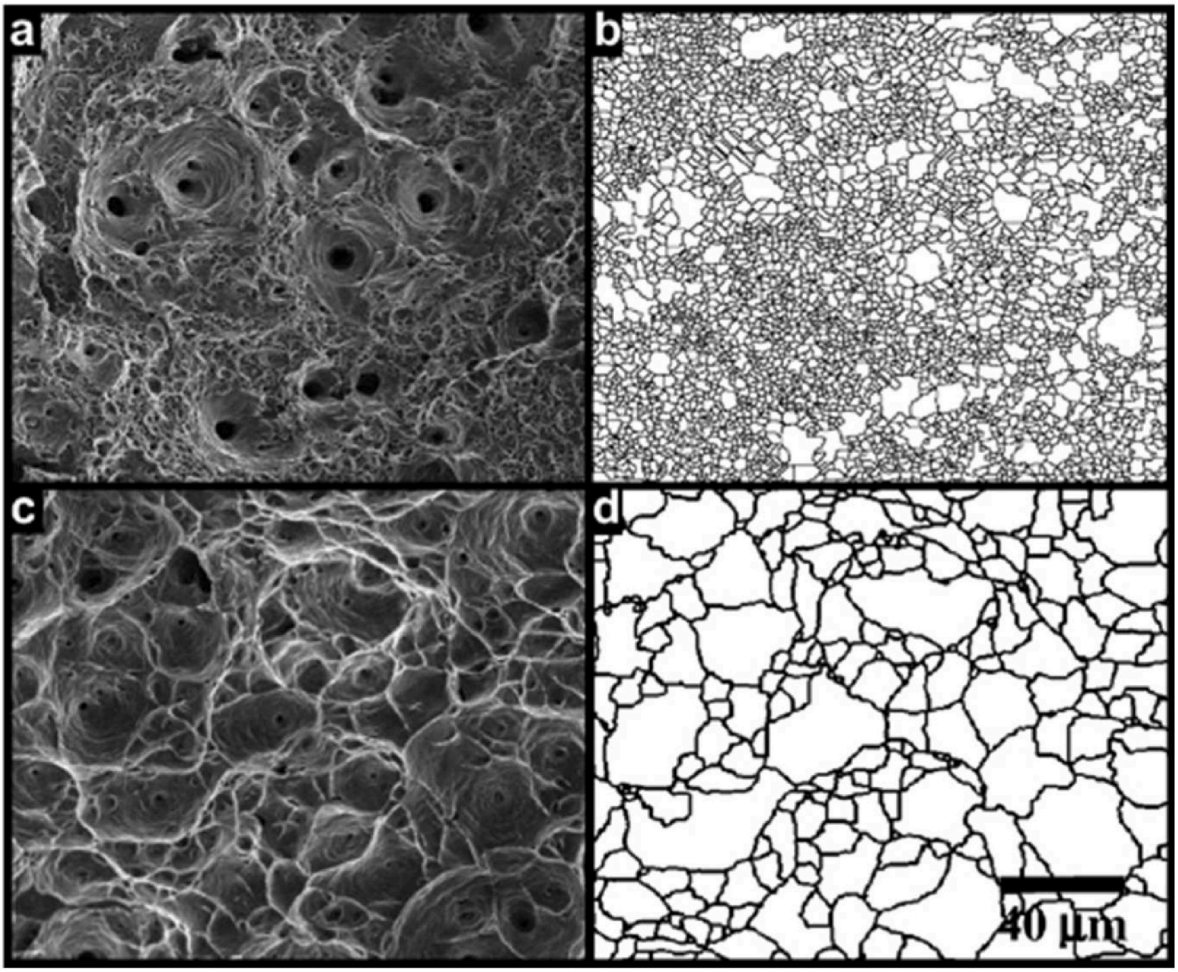

Fig. 14. Correlation of ductile fracture and grain size in structural steels for: (a) SEM−SE image of mainly small dimples and (b) corresponding void networks of relatively small grains, (c) SEM−SE image of mainly large dimples and d) corresponding void networks of large grains (where (b) and (d) are outputs from advanced image processing [138]).

that 0.13 wt% vanadium is optimal for cost-performance efficiency, aligning with sustainability objectives.

The ductile-to-brittle transition temperature (DBTT) of the vanadium-microalloyed steels ranged from −50°C to 200°C. This shows the impact of heat treatment on toughness and transition behavior. The Charpy V-notch impact energy decreased with decreasing temperatures, a typical transition from ductile to brittle fracture. Steels normalised and furnace-cooled exhibited lower DBTT values and higher impact toughness compared to quenched and tempered steels, emphasizing their superior balance of toughness and strength. The ferrite-bainite microstructures in normalised steels contributed to their improved low-temperature toughness, while the tempered martensitic structure in quenched steels resulted in higher DBTT and reduced toughness. These findings demonstrate the critical role of optimizing heat treatment processes and microstructure to tailor the mechanical properties of microalloyed steels for rail axle applications, where resistance to brittle fracture is crucial for structural integrity, reliability and safety.

Finally, the 0 wt% V and 0.13 wt% V alloys exhibit a promising combination of strength, ductility, and toughness for rail axle applications, outperforming traditional ferrite-pearlite steels. The findings indicate that these micro-alloyed steels not only meet but exceed global standards, providing a sustainable and cost-effective solution for modern rail axle design. Further optimization based on these results could facilitate enhanced material performance while maintaining economic feasibility.

CRediT authorship contribution statement

D.E.P. Klenam: Writing – review & editing, Writing – original draft, Software, Methodology, Investigation, Formal analysis, Conceptualization. **L.H. Chown:** Writing – review & editing, Supervision, Software, Resources, Project administration, Conceptualization. **M.J. Papo:** Writing – review & editing, Supervision, Resources. **L.A. Cornish:** Writing – review & editing, Supervision, Software, Resources, Project administration, Conceptualization.

Declaration of competing interest

The authors declare that they have no known competing financial interests or personal relationships that could have appeared to influence the work reported in this paper.

Acknowledgements

The support from the Department of Science and Innovation (DSI), the National Research Foundation (NRF) and Advanced Materials Division, Mintek are gratefully acknowledged.

References

[1] G. Dubois, B. Sovacool, C. Aall, M. Nilsson, C. Barbier, A. Herrmann, S. Bruyère, C. Andersson, B. Skold, F. Nadaud, F. Dorner, K.R. Moberg, J.P. Ceron, H. Fischer,

D. Amelung, M. Baltruszewicz, J. Fischer, F. Benevise, V.R. Louis, R. Sauerborn, Energy Res. Social Sci. 52 (2019) 144–158.
[2] D. Raabe, Chem. Rev. 123 (2023) 2436–2608.
[3] J.L. Cann, A. De Luca, D.C. Dunand, D. Dye, D.B. Miracle, H.S. Oh, E.A. Olivetti, T.M. Pollock, W.J. Poole, R. Yang, C.C. Tasan, Prog. Mater. Sci. 117 (2020) 100722.
[4] D. Raabe, C.C. Tasan, E.A. Olivetti, Nature 575 (2019) 64–74.
[5] J.X. Guo, Y. Zeng, K. Zhu, X. Tan, Sci. Total Environ. 785 (2021) 147264.
[6] P. Verma, T. Kumari, A.S. Raghubanshi, Renew. Sustain. Energy Rev. 147 (2021) 111210.
[7] R.A. Smith, Europ. Struct. Integ. Soc. 26 (2000) 173–181.
[8] M. Luke, I. Varfolomeev, K. Lütkepohl, A. Esderts, Eng. Fail. Anal. 17 (2010) 617–623.
[9] M. Luke, I. Varfolomeev, K. Lütkepohl, A. Esderts, Eng. Fract. Mech. 78 (2011) 714–730.
[10] Japanese Industrial Standards, Standard E4501. Railway Rolling Stock - Design Method for Strength of Axles, 1995.
[11] J. Rudlin, D. Panggabean, A. Loconte, A. Raude, 51st Annual Conference of the British Institute of Non-destructive Testing 2012, NDT 2012, 2012, pp. 63–69.
[12] D.E.P. Klenam, L.H. Chown, M.J. Papo, L.A. Cornish, Crit. Rev. Solid State Mater. Sci. 49 (2022) 163–193.
[13] S. Beretta, U. Zerbst, Eng. Fract. Mech. 78 (2011) 713.
[14] European Standard, EN 13261. Railway Applications - Wheelsets and Bogies - Axles - Product Requirement, Annex A, European Committee for Standardization (CEN), Brussels, Belgium, 2003.
[15] European Standard, EN 13103. Railway Applications - Wheelsets and Bogies - Non Powered Axles - Design Method, European Committee for Standardization (CEN), Brussels, Belgium, 2001.
[16] M. Filippini, M. Luke, I. Varfolomeev, D. Regazzi, S. Beretta, Procedia Struct. Integr. 4 (2017) 11–18.
[17] U. Zerbst, M. Schödel, H.Th Beier, Eng. Fract. Mech. 78 (2011) 793–809.
[18] U. Zerbst, R. Lundén, K.-O.O. Edel, R.A.A. Smith, Eng. Fract. Mech. 76 (2009) 2563–2601.
[19] A.P. Moon, S. Sangal, S. Srivastav, N.S. Gajbhiye, K. Mondal, J. Mater. Eng. Perform. 24 (2015) 85–97.
[20] U. Zerbst, S. Beretta, G. Köhler, A. Lawton, M. Vormwald, H. Th, T. Beier, C. Klinger, I. Černý, J. Rudlin, T. Heckel, D. Klingbeil, Eng. Fract. Mech. 98 (2013) 214–271.
[21] U. Zerbst, M. Madia, C. Klinger, D. Bettge, Y. Murakami, Eng. Fail. Anal. 97 (2019) 759–776.
[22] A. Moon, S. Sangal, K. Mondal, Indian Metals 66 (1) (2013) 33–41.
[23] J.W. Gao, G.Z. Dai, Q.Z. Li, M.N. Zhang, S.P. Zhu, J.A.F.O. Correia, G. Lesiuk, A. M.P. De Jesus, Int. J. Fatig. 146 (2021).
[24] J.A. Balbín, V. Chaves, N.O. Larrosa, Corrosion Sci. 180 (2021) 109171.
[25] Y. Hu, S. Wu, P.J. Withers, H. Cao, P. Chen, Y. Zhang, Z. Shen, T. Vojtek, P. Hutař, Eng. Fract. Mech. 245 (2021) 107588.
[26] U. Zerbst, C. Klinger, D. Klingbeil, Eng. Fail. Anal. 35 (2013) 54–65.
[27] G. Epasto, F. Distefano, L. Gu, H. Mozafari, E. Linul, Mater. Des. 196 (2020) 109120.
[28] X. Zhao, S. Wu, J. Bao, N. Ao, W. Peng, W. Sun, Eng. Fail. Anal. 125 (2021).
[29] J.W. Gao, M.H. Yu, D. Liao, S.P. Zhu, Z.Y. Zhu, J. Han, Mater. Des. 202 (2021) 109488.
[30] U. Zerbst, M. Madia, C. Klinger, D. Bettge, Y. Murakami, Eng. Fail. Anal. 98 (2019) 228–239.
[31] S. Foletti, S. Beretta, G. Gurer, Int. J. Fatig. 86 (2016) 34–43.
[32] A. Amini, M. Entezami, M. Papaelias, Case Stud. Nondestruct. Test. Eval. 6 (2016) 8–16.
[33] B.C. Goo, H.S. Mun, I.S. Cho, Appl. Sci. (2020) 10.
[34] R. Luo, W. Teng, X. Wu, H. Shi, J. Zeng, Veh. Syst. Dyn. 58 (2020) 1914–1934.
[35] J.W. Gao, M.H. Yu, D. Liao, S.P. Zhu, J. Han, G. Lesiuk, J.A.F.O. Correia, A.M. P. De Jesus, Int. J. Fatig. 149 (2021) 106276.
[36] A. Landaberea, I. Irizar, Proceedings of 2016 IEEE International Wheelset Congress, IWC 2016, 2017, pp. 111–116.
[37] Ř. Bohuslav, V. Jaroslav, N. Tomáš, Residual Stresses 2018, vol. 6, 2018, pp. 95–100.
[38] J.L. Lanzagorta, I. Aizpurua, P.R. Vázquez, I. Castro, NDT E Int. 121 (2021).
[39] X. Wang, L. Chen, P. Liu, G. Lin, X. Ren, Metals 10 (2020) 1–14.
[40] T. Li, W. Sun, Z. Meng, J. Huo, J. Dong, L. Wang, Adv. Mech. Eng. 11 (2019) 1–13.
[41] C. Li, W. Dai, H. Zhang, Y. Liu, Y. Zhang, Eng. Fract. Mech. 238 (2020) 107287.
[42] L. Paties, Minimizing the Risk of Fatigue Failure of Railway Axles, 2014. Belgium.
[43] D.E.P. Klenam, Composition Refinement of Medium Carbon-Low Alloy Steels to Improve Wear and Corrosion Resistance for Rail Axle Applications, University of the Witwatersrand, 2019.
[44] J.W. Zhang, Y.G. Cao, C.G. Zhang, Z.D. Li, W.X. Wang, J. Iron Steel Res. Int. 29 (2021) 802–809.
[45] E. Schmidová, P. Paščenko, B. Culek, M. Schmid, Eng. Fail. Anal. 123 (2021) 105253.
[46] C. Zhang, Q. Wang, J. Ren, R. Li, M. Wang, F. Zhang, K. Sun, Mater. Sci. Eng. 534 (2012) 339–346.
[47] Y. Zou, J. Li, X. Liu, T. He, J. Lu, D. Li, Y. Li, Surf. Coat. Technol. 412 (2021) 127012.
[48] U. Zerbst, M. Schödel, R. Heyder, Eng. Fract. Mech. 76 (2009) 2637–2653.
[49] D. Jorge-Badiola, A. Iza-Mendia, B. Lopez, J.M. Rodriguez-Ibabe, ISIJ Int. 49 (2009) 1615–1623.
[50] X. Zhang, S. Liu, K. Wang, L. Yan, J. Wang, Q. Xia, H. Yu, Mater. Sci. Eng., A 884 (2023) 145578.
[51] S. Nafisi, M. Arafin, R. Glodowski, L. Collins, J. Szpunar, ISIJ Int. 54 (2014) 2404–2410.
[52] A.G. Kostryzhev, M. Strangwood, C.L. Davis, Metal. Mater. Trans. A Phys. Metal. Mater. Sci. 41 (2010) 1399–1408.
[53] A.G. Kostryzhev, M. Strangwood, C.L. Davis, Ironmaking and Steelmaking, vol. 36, 2009, pp. 186–192.
[54] T. Siwecki, J. Eliasson, R. Lagneborg, B. Hutchinson, ISIJ Int. 50 (2010) 760–767.
[55] N. Bi, H. Tang, Z. Shi, X. Wang, F. Han, J. Liang, Materials 16 (6) (2023) 2220.
[56] H.H. Jin, C.S. Shin, H.C. Lee, Solid State Phenom. 135 (2008) 111–114.
[57] A. Kaynar, S. Gündüz, M. Türkmen, Mater. Des. 51 (2013) 819–825.
[58] H. lian Wei, G. quan Liu, H. tao Zhao, M. he Zhang, Mater. Sci. Eng., A 596 (2014) 112–120.
[59] S. Shanmugam, R.D.K. Misra, T. Mannering, D. Panda, S.G. Jansto, Mater. Sci. Eng., A 437 (2006) 436–445.
[60] S. Gündüz, R.C. Cochrane, Mater. Des. 26 (2005) 486–492.
[61] W., B.X. Xingui Liu, Yi, in: HSLA Steels 2015, Microalloying 2015 & Offshore Engineering Steels 2015, Springer International Publishing, Cham, 2016, pp. 1027–1033.
[62] K. He, D.V. Edmonds, Mater. Sci. Technol. 18 (2002) 289–296.
[63] K.S. Kim, L.X. Du, C.R. Gao, Acta Metall. Sin. 28 (2015) 692–698.
[64] T.N. Baker, Ironmak. Steelmak. 43 (2016) 264–307.
[65] T.N. Baker, Mater. Sci. Technol. 25 (2009) 1083–1107.
[66] Z. Ye, C. Li, X. Zhang, Y. Liao, J. Gu, Mater. Char. 192 (2022).
[67] K.-T. Park, Y.-S. Kim, D.H. Shin, Microstructural Stability of Ultrafine Grained Low-Carbon Steel Containing Vanadium Fabricated by Intense Plastic Straining, n.d.
[68] D.H. Shin, J. Park, S.Y. Chang, Y. Lee, K. Park, ISIJ Int. 42 (2002) 1490–1496.
[69] A.J.P. Gater, G. Fourlaris, S.G.R. Brown, L.J. Baker, Ironmaking and Steelmaking, vol. 39, 2012, pp. 216–221.
[70] D.Y. Shin, C.H. Wee, M.S. Kim, B.D. You, J.W. Han, S.O. Choi, D.J. Yun, Distribution Behavior of Vanadium and Phosphorus between Slag and Molten Steel, 2007.
[71] Y. Ohmori, Trans. ISIJ Int. 11 (1971) 1160–1165.
[72] P.C.M. Rodrigues, E. V Pereloma, D.B. Santos, Mechanical Properities of an HSLA Bainitic Steel Subjected to Controlled Rolling with Accelerated Cooling, 2000.
[73] A.B. Cota, R. Barbosa, D.B. Santos, J. Mater. Process. Technol. 100 (2000) 156–162.
[74] M. Thompson, M. Ferry, P.A. Manohar, ISIJ Int. (2001) 891–899.
[75] J.R. Snell, Proc. Inst. Mech. Eng. F J. Rail Rapid Transit 218 (2004) 279–282.
[76] ASTM International, ASTM E92 - 17: Standard Test Methods for Vickers Hardness and Knoop Hardness of Metallic Materials, 1999.
[77] M. Novosad, R. Fajkoš, B. Řeha, R. Řezníček, in: Procedia Eng, 2010, pp. 2259–2268.
[78] G. Mancini, A. Corbizi, F. Lombardo, S. Cervello, in: Proceedings of World Congress on Railway Research, 2006, pp. 1–12.
[79] R.O. Ritchie, Nat. Mater. 10 (2011) 817–822.
[80] D.E.P. Klenam, L.H. Chown, M.J. Papo, L.A. Cornish, MRS Adv. 3 (2018) 2169–2181.
[81] F. Dikmen, M. Bayraktar, R. Guclu, Strojniški vestnik, J. Mech. Eng. 58 (2012) 545–552.
[82] S. Beretta, M. Carboni, S. Cervello, Mater. Werkst. 42 (2011) 1099–1104.
[83] T. Makino, H. Sakai, C. Kozuka, Y. Yamazaki, M. Yamamoto, K. Minoshima, Int. J. Fatig. 132 (2020) 105361.
[84] G. Krauss, Mater. Sci. Eng. 273–275 (1999) 40–57.
[85] D. Klingbeil, U. Zerbst, C. Klinger, in: 13th International Conference on Fracture, 2013. Beijing, China.
[86] U. Zerbst, C. Klinger, R. Clegg, Eng. Fail. Anal. 55 (2015) 376–410.
[87] U. Zerbst, S. Beretta, Eng. Fail. Anal. 18 (2011) 534–542.
[88] C. Lonsdale, D. Stone, Proc. Inst. Mech. Eng. F J. Rail Rapid Transit 218 (2004) 293–298.
[89] V. Grubisic, G. Fischer, Proc. Inst. Mech. Eng. F J. Rail Rapid Transit 226 (2012) 518–529.
[90] V. Linhart, I. Černý, Eng. Fract. Mech. 78 (2011) 731–741.
[91] S. Beretta, M. Carboni, G. Fiore, A. Lo Conte, Int. J. Fatig. 32 (2010) 952–961.
[92] H.K.D.H. Bhadeshia, Acta Metall. 28 (1980) 1103–1114.
[93] P.J. Withers, H.K.D.H. Bhadeshia, Mater. Sci. Technol. 17 (2001) 355–365.
[94] F.G. Caballero, H.K.D.H. Bhadeshia, K.J.A. Mawella, D.G. Jones, P. Brown, Mater. Sci. Technol. 17 (2001) 512–516.
[95] S. Dépinoy, B. Marini, C. Toffolon-Masclet, F. Roch, A.F. Gourgues-Lorenzon, Metal. Mater. Trans. A Phys. Metal. Mater. Sci. 48 (2017) 2289–2300.
[96] M. Ramajayam, N. Stanford, Mater. Sci. Eng. 671 (2016) 147–157.
[97] M.J. Santofimia, L. Zhao, J. Sietsma, Metal. Mater. Trans. A Phys. Metal. Mater. Sci. 40 (2009) 46–57.
[98] M. Gensamer, E.B. Pearsall, W.S. Pellini, J.R. Low, Metallogr. Microstruct. Anal. 1 (2012) 171–189.
[99] A.F. Gourgues, H.M. Flower, T.C. Lindley, Mater. Sci. Technol. 16 (2000) 26–40.
[100] J.C.F. Jorge, L.F.G.D. Souza, M.C. Mendes, I.S. Bott, L.S. Araújo, V.R.D. Santos, J. M.A. Rebello, G.M. Evans, J. Mater. Res. Technol. 10 (2021) 471–501.
[101] E.O. Hall, Proc. Phys. Soc. B 64 (1951) 747–753.
[102] B.B. He, M.X. Huang, Metal. Mater. Trans. A Phys. Metal. Mater. Sci. 46 (2015) 688–694.
[103] T.K. Asumadu, K. Mensah-Darkwa, E. Gikunoo, D.E.P. Klenam, M. Vandadi, N. Rahbar, S. Kwofie, W.O. Soboyejo, Mater. Sci. Eng., A 871 (2023).
[104] R.A. Grange, Metall. Trans. A 2 (1971) 65–78.

[105] M. Shamsujjoha, Mater. Sci. Eng., A 776 (2020).
[106] G. Shi, H. Zhao, S. Zhang, Q. Wang, F. Zhang, Mater. Sci. Eng., A 769 (2020).
[107] R. Lagneborg, B. Hutchinson, T. Siwecki, S. Zajac, The Role of Vanadium in Microalloyed Steels, Swerea KIMAB, Sweden, 2014.
[108] B.D. Cullity, Element of X-Ray Diffraction, second ed., Addison-Wesley, Reading, 1978.
[109] H. Yu, F. Guo, Y. Ma, Y. Wang, X. Li, K. Li, L. Jiang, H. Liu, J. Alloys Compd. (2024) 174188.
[110] C. Shi, X. Zhu, X. Zheng, P. Lan, J. Li, Mater. Sci. Eng., A 854 (2022).
[111] J. Xie, X.P. Chen, Y. Cao, G.J. Huang, Q. Liu, Mater. Des. 221 (2022).
[112] S. Fu, P. Liu, X. Chen, H. Zhou, F. Ma, W. Li, K. Zhang, Mater. Sci. Eng., A 802 (2021).
[113] M. Eissa, K. El-Fawakhry, M. Mekkawy, A.H. Hussein, A. Tawfik, Steel Res. 69 (1998) 334–342.
[114] H.K.D.H. Bhadeshia, Acta Metall. 29 (1981) 1117–1130.
[115] H.K.D.H. Bhadeshia, M. Déchamps, L.M. Brown, Acta Metall. 29 (1981) 1473–1474.
[116] D. Biermann, H. Hartmann, I. Terwey, C. Merkel, D. Kehl, Procedia CIRP 7 (2013) 276–281.
[117] J. Kalousek, D.M.M. Fegredo, E.E.E. Laufer, Wear 105 (1985) 199–222.
[118] G.G. Ribamar, J.D. Escobar, A. Kwiatkowski da Silva, N. Schell, J.A. Ávila, A. S. Nishikawa, J.P. Oliveira, H. Goldenstein, Acta Mater. 247 (2023).
[119] N. Gorain, M.G. Walunj, M.K. Soni, B.R. Kumar, Arch. Civ. Mech. Eng. 20 (2020).
[120] V.H. Baltazar Hernandez, S.S. Nayak, Y. Zhou, Metall. Mater. Trans. 42 (2011) 3115–3129.
[121] J. Teixeira, M. Moreno, S.Y.P. Allain, C. Oberbillig, G. Geandier, F. Bonnet, Acta Mater. 212 (2021) 116920.
[122] S. Breumier, T. Martinez Ostormujof, B. Frincu, N. Gey, A. Couturier, N. Loukachenko, P.E. Aba-perea, L. Germain, Mater. Char. 186 (2022) 111805.
[123] I. Gutiérrez, Mater. Sci. Eng. 571 (2013) 57–67.
[124] W. Xiong, R. Song, W. Huo, P. Yu, S. Qin, Z. Liu, Vacuum 195 (2022) 110709.
[125] P.K. Katiyar Neetu, S. Sangal, K. Mondal, Corrosion Sci. 178 (2021) 109043.
[126] F.H. Samuel, D. Daniel, O. Sudre, Mater. Sci. Eng. 92 (1987) 43–62.
[127] S. Zaefferer, J. Ohlert, W. Bleck, Acta Mater. 52 (2004) 2765–2778.
[128] R.A. Grange, Metall. Trans. A 2 (1971) 417–426.
[129] S. Cantini, G. Patelli, S. Beretta, M. Carboni, (2009) 21–22.
[130] S. Hillmansen, Proc. Inst Mech Eng Part F: J Rail Rapid Transit, vol. 218, 2004.
[131] F. Yang, H. Luo, E. Pu, S. Zhang, H. Dong, Int. J. Plast. 103 (2018) 188–202.
[132] A. Yilmaz, Sci. Technol. Adv. Mater. 12 (2011).
[133] P.G. Mccormick, Acta Metall. 21 (1973) 873–878.
[134] A. Sarkar, A. Chatterjee, P. Barat, P. Mukherjee, Mater. Sci. Eng., A 459 (2007) 361–365.
[135] E.O. Hall, J. Mech. Phys. Solid. 1 (1953) 227–233.
[136] P. Maruschak, I. Konovalenko, O. Prentkovskis, O. Tsyrulnyk, in: Procedia Eng, Elsevier Ltd, 2016, pp. 437–442.
[137] W. Qin, J. Li, Y. Liu, J. Kang, L. Zhu, D. Shu, P. Peng, D. She, D. Meng, Y. Li, Mater. Lett. 254 (2019) 116–119.
[138] A. Das, S. Tarafder, Scripta Mater. 59 (2008) 1014–1017.
[139] L. Sanz, B. Pereda, B. López, Mater. Sci. Eng., A 685 (2017) 377–390.
[140] N. Kamikawa, K. Sato, G. Miyamoto, M. Murayama, N. Sekido, K. Tsuzaki, T. Furuhara, Acta Mater. 83 (2015) 383–396.
[141] X. Li, Y. Wei, L. Lu, K. Lu, H. Gao, Nature 464 (2010) 877–880.
[142] T. Gladman, Mater. Sci. Technol. 15 (1999) 30–36.
[143] K.S. Chan, Metall. Trans. A 23 (1992) 183–199.
[144] D.E.P. Klenam, J.E. Oghenevweta, W.O. Soboyejo, in: Comprehensive Structural Integrity, Elsevier, 2023, pp. 102–139.
[145] K.S. Chan, Metall. Mater. Trans. 25 (1994) 299–308.
[146] J.R. Greer, J.T.M. De Hosson, Prog. Mater. Sci. (2011) 654–724.
[147] R.O. Ritchie, Int. J. Fract. 100 (1999) 55–83.
[148] R.O. Ritchie, Phil. Trans. Math. Phys. Eng. Sci. 379 (2021).
[149] J. Lou, W.O. Soboyejo, Metal. Mater. Trans. A Phys. Metal. Mater. Sci. 32 (2001) 325–337.
[150] Association of American Railroads, Manual of Standards and Recommended Practices - Section G, Wheels and Axles, 2007. Specification M107/208, Wheels, Carbon Steels, Washington, D.C. USA.
[151] Q. Yuan, J. Ren, J. Mo, Z. Zhang, E. Tang, G. Xu, Z. Xue, J. Mater. Res. Technol. 23 (2023) 3756–3771.
[152] H. Hu, G. Xu, L. Wang, Z. Xue, Y. Zhang, G. Liu, Mater. Des. 84 (2015) 95–99.
[153] M. Žaludová, B. Smetana, S. Zlá, J. Dobrovská, A. Watson, J. Vontorová, S. Rosypalová, J. Kukutschová, M. Cagala, J. Therm. Anal. Calorim. 112 (2013) 465–471.
[154] M. Bleckmann, J. Gleinig, J. Hufenbach, H. Wendrock, L. Giebeler, J. Zeisig, U. Diekmann, J. Eckert, U. Kühn, J. Alloys Compd. 634 (2015) 200–207.
[155] S.E. Offerman, N.H. Van Dijk, M.T. Rekveldt, J. Sietsma, S. Van der Zwaag, Mater. Sci. Technol. 18 (2002) 297–303.
[156] F.G. Caballero, A. García-Junceda, C. Capdevila, C.G. De Andrés, Mater. Trans. 47 (2006) 2269–2276.
[157] B.L. Ennis, C. Bos, M.P. Aarnts, P.D. Lee, E. Jimenez-Melero, Mater. Sci. Eng., A 713 (2018) 278–286.
[158] T.B. Cox, J.R. Low, Metall. Trans. A 5 (1974) 1457–1470.
[159] J.W. Hancock, A.C. Mackenzie, J. Mech. Phys. Solid. 24 (1976) 147–169.
[160] G.T. Hahn, A.R. Rosenfield, Metall. Trans. A 6 (1975) 653–668.
[161] D. Broek, Eng. Fract. Mech. 5 (1913) 55–66.
[162] A. Pineau, A.A. Benzerga, T. Pardoen, Acta Mater. 107 (2016) 424–483.
[163] J.H. Shim, Y.J. Oh, J.Y. Suh, Y.W. Cho, J.D. Shim, J.S. Byun, D.N. Lee, Acta Mater. 49 (2001) 2115–2122.